

A Geometric Framework for Stiffness Mappings of Compliant Robotic Systems on the Special Euclidean Group

Tengyu Hou ^{1b}, Ye Ding ^{1b}, *Member, IEEE*, and Xiangyang Zhu ^{1b}, *Member, IEEE*

Abstract—In this article, the stiffness mapping of compliant robotic systems is generalized to the special Euclidean group SE(3). A geometric framework is proposed to unify the existing stiffness models. We analyze the symmetry and exactness relationship between joint and Cartesian stiffness matrices in this framework. To verify the theoretical results, motions of different types of manipulators, including serial and parallel ones, are tested in simulations. Based on the conservative property of the stiffness matrix, an impedance control strategy to achieve variable stiffness is proposed. In addition, a feasible stiffness identification method is developed using the skew-symmetric structure of the stiffness matrix.

Index Terms—Conservative stiffness matrix, impedance control, passivity-based control, stiffness identification, stiffness mapping, symmetry and exactness.

I. INTRODUCTION

ROBOT stiffness describes the amount of deflection that occurs when the end-effector is subjected to an external force. In applications such as robotic processing and gripping, the design or control of appropriate stiffness parameters largely determines the performance of the compliant robotic system as the robot interacts with the environment. Therefore, robot stiffness modeling has become a fundamental and critical issue.

In the early work, Dimentberg [1] used the screw theory developed by Ball [2] to describe the moving rigid body in the potential field, further giving the symmetric stiffness matrix in the equilibrium state. With the help of the Lie algebra, Loncaric [3] studied the system of single rigid bodies connected by a linear spring, giving the properties of the stiffness matrix.

The current mainstream stiffness modeling methods are roughly divided into the finite element analysis (FEA) method [4], [5], [6], [7], the matrix structural analysis (MSA) method [8], [9], [10], [11], and the virtual joint modeling (VJM) method [12], [13], [14], [15], [16]. Compared with the FEA and MSA, as shown in Fig. 1, the VJM unifies the flexibility of the

actuator, linkage, and other components into a flexible virtual spring and maps the flexibility characterized by the virtual spring to the end-effector of the robot system. The VJM represents a more clear physical model and is much less computationally intensive, so it has been widely used in stiffness modeling and has been developed over the years. Salisbury [17] considered the flexibility mainly originates from the actuator and treated the links as rigid bodies, deriving the conventional stiffness mapping $\mathbf{K}_C = \mathbf{J}^{-T} \mathbf{K}_\theta \mathbf{J}^{-1}$ for the serial manipulator to describe the stiffness transformation between Cartesian space and joint space. Here, \mathbf{K}_θ is the stiffness matrix corresponding to the virtual spring, \mathbf{K}_C is the Cartesian stiffness matrix of the robotic end-effector characterization, and \mathbf{J} is the kinematic Jacobian. Gosselin [18] further generalized Salisbury's model and showed that the stiffness mapping has a similar form on parallel manipulators. Zhang et al. [19], [20] included the flexibility of the actuators and connecting rods to model the stiffness of serial and parallel manipulators. Pashkevich et al. [12] expressed the flexibility of the linkage in terms of a six-dimensional spring and considered the effect of the passive joint on the stiffness of the serial and parallel manipulators. Chen and Kao [21] took into account the loads applied to the end-effector of the serial manipulator and derived conservative congruence transformation (CCT) $\mathbf{K}_C = \mathbf{J}^{-T} (\mathbf{K}_\theta - \mathbf{K}_g) \mathbf{J}^{-1}$. \mathbf{K}_g describes the effect on the system stiffness due to external forces as well as changes in the Jacobian. When the manipulator is not subjected to the external load, the stiffness component \mathbf{K}_g is zero, and the stiffness mapping relationship degenerates to the case of conventional stiffness transformation. In addition, Kao et al. [22] pointed out that CCT is still valid for parallel manipulators. Alici and Shirinzadeh [23] experimentally illustrated the correctness of CCT. A more general mapping of stiffness $\mathbf{K}_C = \mathbf{J}^{-T} (\mathbf{K}_\theta - \mathbf{K}_g + \mathbf{K}_I) \mathbf{J}^{-1}$ was obtained by Quennouelle and Gosselin [14], [24], [25] by including the external forces on the mechanical system as well as geometric constraints. In this case, \mathbf{K}_I is induced by geometric constraints and passive joints. Yi and Freeman [26], [27] took external loads, gravity loads, and drive redundancy into account to obtain the nonlinear stiffness model. Subsequently, more and more factors were considered in the stiffness modeling. Pashkevich et al. [13] performed nonlinear stiffness modeling of manipulators subjected to external and internal loads with passive joints and successfully predicted nonlinear behavior such as buckling. Later, they considered more types of external as well as internal loads to refine the nonlinear

Manuscript received 22 March 2023; revised 31 July 2023; accepted 29 September 2023. Date of publication 29 November 2023; date of current version 15 March 2024. This article was recommended for publication by Associate Editor Qinchuan Li and Editor Eiichi Yoshida upon evaluation of the reviewers' comments. This work was supported by the National Natural Science Foundation of China under Grant 51822506 and Grant 51935010. (*Corresponding author: Ye Ding.*)

The authors are with the State Key Laboratory of Mechanical System and Vibration, School of Mechanical Engineering, Shanghai Jiao Tong University, Shanghai 200240, China (e-mail: htyhtyhty@sjtu.edu.cn; y.ding@sjtu.edu.cn; mexyzhu@sjtu.edu.cn).

Digital Object Identifier 10.1109/TRO.2023.3323824



Fig. 1. Compliant robotic systems. The yellow virtual springs characterize the flexibility of the system in joint space, and the red virtual springs characterize the flexibility of the system in Cartesian space as it interacts with the environment. (a) The serial manipulator with virtual springs. (b) The parallel manipulator with virtual springs.

stiffness model [16]. It is worth mentioning that the actual factors considered in the various stiffness modeling methods mentioned above are different, and their corresponding stiffness transformation relations are also slightly different. Meanwhile, the VJM has been widely used to model the stiffness of specific serial and parallel manipulators [28], [29], [30], [31], [32], [33], [34].

The stiffness properties characterized by the mechanical system have received lots of attention. Griffis and Duffy [35] studied the planar and spatial spring system by modeling the stiffness mapping at the point of deviation from the equilibrium and showed that the stiffness matrix is asymmetric. The stiffness matrix can be approximated as a symmetric matrix when the system is near equilibrium. Ciblak and Lipkin [36] showed that the stiffness matrix becomes asymmetric in the presence of external forces and gave an analytical expression for the skew-symmetric part of the stiffness matrix. The symmetry of the stiffness matrix was explained in terms of energy interaction with the environment in robotic grasping by Li and Kao [37]. Pigoski et al. [38] gave the coordinate system that makes the stiffness matrix a symmetric matrix. Howard et al. [39] reached a similar conclusion by using differential geometry. However, they did not reveal the relationship between geometry and stiffness mapping. Although modeling of the stiffness matrix in nonequilibrium states had been previously available [26], [40], [41], Chen and Kao [21], Kao and Ngo [42], Chen [43] first systematically studied the properties of the stiffness matrix under the action of external forces from the perspective of conservative properties. They pointed out that \mathbf{K}_C satisfies both exactness and symmetry under the CCT in linear $\mathbb{R}^{3 \times 3}$ spaces. However, they basically elaborate properties from a qualitative perspective. Žefran and Kumar [44] used differential geometry to model the stiffness tensor and showed that the connection determines the symmetry of the stiffness tensor. The symmetric connection will result in a symmetric stiffness matrix. Other works analyzed the properties of the stiffness matrix from different perspectives [45], [46], [47].

From the existing literature review, it is known that stiffness modeling is often done from a mechanical point of view: when the considered mechanical conditions change, the established stiffness models change, which leads to difficulties in obtaining

a uniform stiffness model. Many researchers study the stiffness matrices in flat space, which often has a complicated and tedious derivation process and unclear geometric intuition. Although there is some work on stiffness modeling using geometric tools, no clear correspondence between the geometric structure and the stiffness mapping has been established. Moreover, a systematic discussion on the property relationship between joint and Cartesian stiffness matrices is lacking. Most of the studies focus on symmetry, and there are few studies on exactness.

This article proposes a geometric framework for describing the stiffness of compliant robotic systems. We give the geometric description of the conservative stiffness matrix using the differential form. Conditions of the conservative stiffness matrix on the translational subgroup $T(3)$ are derived by considering symmetry and exactness. We further generalize the conclusion to $SE(3)$: a symmetric and exact joint stiffness matrix corresponds to a conservative Cartesian stiffness matrix. Unlike the commonly used mechanical perspective, the geometric structures behind the different stiffness mappings are revealed. Then, we introduce some stiffness mappings with specific properties, where CCT is the only transformation to generate conservative Cartesian stiffness matrices on $T(3)$. In addition, we derive the exact congruence transformation (ECT), which produces exact stiffness matrices on $T(3)$. All the stiffness mapping models can be unified in the differential geometry framework. Finally, the above analysis of exactness and symmetry guides the impedance controller's design and the stiffness matrix's identification.

The contributions of this article can be summarized as follows.

- 1) We use the stiffness tensor defined on the manifold to unify the stiffness models from the above literature in a differential geometry framework, as shown in Table III. In the geometric framework, the properties of the stiffness matrix can be clearly explored.
- 2) We quantitatively derive the correspondence of the properties of the joint stiffness matrix to the properties of the Cartesian stiffness matrix on $T(3)$. Further, we generalize the conclusion to $SE(3)$: a symmetric and exact joint stiffness matrix corresponds to a conservative Cartesian stiffness matrix under CCT, as shown in Fig. 3. This further shows

that a Cartesian matrix can still be conservative when it is not symmetric and exact on $SE(3)$.

- 3) Using the conservative property of the stiffness matrix, we design an impedance control strategy that allows generating a variable stiffness while maintaining passivity. Meanwhile, by analyzing the symmetry of the stiffness matrix, we propose a feasible stiffness identification strategy.

The rest of the article is organized as follows. Section II introduces the background knowledge about differential geometry and stiffness matrix. The relevant notations are summarized in Table I. For more specialized and detailed content, readers can refer to [48], [49], [50], [51]. Then, the conditions for conservative stiffness matrix on $T(3)$ are given in Section III, and the relationship between the joint and Cartesian stiffness matrices on $T(3)$ will also be given in this section. In Section IV, the geometry corresponding to CCT is presented and used to analyze the properties of Cartesian stiffness matrices. Meanwhile, the conclusion about the conservative stiffness matrix is extended to $SE(3)$. A class of stiffness mappings with special properties is presented in Section V, and the correspondence between the geometry and the stiffness mapping is revealed. In Section VI, the validity of the previous theory results is illustrated using serial and parallel manipulator simulations. The selection of connection for practical situations and two specific applications of the aforementioned theory are illustrated in Section VII. Finally, Section VIII concludes this article.

II. BACKGROUND KNOWLEDGE

A. Introduction to $SE(3)$

A rigid body moving in space has six degrees of freedom. The special orthogonal group $SO(3)$ can represent the rotation, and \mathbb{R}^3 can represent the translation. The 6-D Lie group formed by the semidirect product of $SO(3)$ with \mathbb{R}^3 becomes $SE(3)$

$$SE(3) = \left\{ \mathbf{A} \mid \mathbf{A} = \begin{bmatrix} \mathbf{R} & \mathbf{d} \\ \mathbf{0} & 1 \end{bmatrix}, \mathbf{d} \in \mathbb{R}^3, \mathbf{R} \in SO(3) \right\}. \quad (1)$$

The identity element on $SE(3)$ is the identity matrix $\mathbf{I}_{4 \times 4}$. The tangent space at $\mathbf{I}_{4 \times 4}$ is called the *Lie algebra* $se(3)$

$$se(3) = \left\{ \begin{bmatrix} \boldsymbol{\Omega} & \mathbf{v} \\ \mathbf{0} & 0 \end{bmatrix}, \boldsymbol{\Omega} \in \mathbb{R}^{3 \times 3}, \mathbf{v} \in \mathbb{R}^3, \boldsymbol{\Omega}^T = -\boldsymbol{\Omega} \right\}. \quad (2)$$

Any element of $se(3)$ can be represented by a 6-D vector after a set of basis is chosen as follows:

$$\mathbf{L}_1 = \begin{bmatrix} 0 & 0 & 0 & 0 \\ 0 & 0 & -1 & 0 \\ 0 & 1 & 0 & 0 \\ 0 & 0 & 0 & 0 \end{bmatrix}, \quad \mathbf{L}_4 = \begin{bmatrix} 0 & 0 & 0 & 1 \\ 0 & 0 & 0 & 0 \\ 0 & 0 & 0 & 0 \\ 0 & 0 & 0 & 0 \end{bmatrix}$$

$$\mathbf{L}_2 = \begin{bmatrix} 0 & 0 & 1 & 0 \\ 0 & 0 & 0 & 0 \\ -1 & 0 & 0 & 0 \\ 0 & 0 & 0 & 0 \end{bmatrix}, \quad \mathbf{L}_5 = \begin{bmatrix} 0 & 0 & 0 & 0 \\ 0 & 0 & 0 & 1 \\ 0 & 0 & 0 & 0 \\ 0 & 0 & 0 & 0 \end{bmatrix}$$

TABLE I
LIST OF NOTATIONS IN THE ARTICLE

| Notation | Explanation |
|--------------------------------|---|
| $SE(3)$ | The special Euclidean group |
| $T(3)$ | The spatial translational subgroup of $SE(3)$ |
| $\mathfrak{X}(SE(3))$ | The set of smooth vector fields on $SE(3)$ |
| $\mathfrak{X}^*(SE(3))$ | The set of smooth dual vector fields on $SE(3)$ |
| $\Omega^k(SE(3))$ | The vector space of smooth k -forms |
| $[\cdot]$ | $:\mathbb{R}^3 \rightarrow so(3)$, The skew-symmetric matrix representation of the vector |
| $[\cdot, \cdot]$ | $:se(3) \times se(3) \rightarrow se(3)$, Lie bracket |
| $\langle \cdot, \cdot \rangle$ | $:\mathfrak{X}^*(SE(3)) \times \mathfrak{X}(SE(3)) \rightarrow \mathbb{R}$, The contraction between the dual vector field and the vector field |
| $\cdot \wedge \cdot$ | $:\Omega^k(SE(3)) \times \Omega^l(SE(3)) \rightarrow \Omega^{k+l}(SE(3))$, The exterior product |
| $d\cdot$ | $:\Omega^k(SE(3)) \rightarrow \Omega^{k+1}(SE(3))$, Exterior differentiation. |
| $R(X, Y) \cdot$ | $:\mathfrak{X}(SE(3)) \rightarrow \mathfrak{X}(SE(3))$, Riemann curvature tensor for given $X, Y \in \mathfrak{X}(M)$ |
| n | $\in \mathbb{N}$, Number of joints |
| Φ | $\in \mathbb{R}$, The potential energy |
| \mathbf{x} | $\in \mathbb{R}^3$, Canonical basis of the Cartesian space $\mathbf{x} = [x, y, z]^T$ or $[x^4, x^5, x^6]^T$ |
| $\boldsymbol{\xi}$ | $\in \mathbb{R}^n$, The joint coordinate vector |
| ξ^i | $\in \mathbb{R}$, The i th joint variable |
| \mathbf{J} | Kinematic Jacobian |
| γ_j^i | $\in \mathbb{R}$, The i th row and j th column of \mathbf{J} |
| α_j^i | $\in \mathbb{R}$, The i th row and j th column of \mathbf{J}^{-1} |
| τ_i | $\in \mathbb{R}$, The torque of i th joint |
| \mathbf{m} | $\in \mathbb{R}^3$, The moment applied at the end-effector |
| \mathbf{f} | $\in \mathbb{R}^3$, The force applied at the end-effector |
| \mathcal{F} | $\in \mathbb{R}^6$, The wrench acting on the end-effector $\mathcal{F} = \begin{bmatrix} \mathbf{m}^T & \mathbf{f}^T \end{bmatrix}^T$ |
| \mathcal{F}_i | $\in \mathbb{R}$, The i th component of the wrench |
| \mathbf{L}_i | $\in se(3)$, The i th basis of $se(3)$ |
| C_{ij}^k | $\in \mathbb{R}$, Structure constants of the Lie algebra |
| $\hat{\mathbf{L}}_i$ | $\in \mathfrak{X}(SE(3))$, The left invariant vector field generated by \mathbf{L}_i |
| $\tilde{\mathbf{L}}_i$ | $\in \mathfrak{X}(SE(3))$, The right invariant vector field generated by \mathbf{L}_i |
| \mathbf{E}_i | $\in \mathfrak{X}(SE(3))$, The coordinate basis vector field $\frac{\partial}{\partial \xi^i}$ |
| ${}^E \Gamma_{ji}^k$ | $\in \mathbb{R}$, The Christoffel symbols under $\{\mathbf{E}_i\}$ |
| ${}^L \Gamma_{ji}^k$ | $\in \mathbb{R}$, The Christoffel symbols under $\{\hat{\mathbf{L}}_i\}$ |
| \mathbf{K}_θ | $\in \mathbb{R}^{n \times n}$, Joint stiffness matrix |
| \mathbf{K}_C | Cartesian stiffness matrix |
| $[\mathbf{K}_\theta]_{ij}$ | $\in \mathbb{R}$, The i th row and j th column of \mathbf{K}_θ |
| $[\mathbf{K}_C]_{ij}$ | $\in \mathbb{R}$, The i th row and j th column of \mathbf{K}_C |
| $K(X, Y)$ | $\in \mathbb{R}$, Components of the stiffness tensor acting on the vector fields X and Y |
| K_{ij}^L | $\in \mathbb{R}$, Components of the stiffness tensor acting on the vector fields $\hat{\mathbf{L}}_i$ and $\tilde{\mathbf{L}}_j$ |
| $\nabla_Y X$ | $\in \mathfrak{X}(SE(3))$, The covariant derivative of X along the direction Y for given $X, Y \in \mathfrak{X}(SE(3))$ |

$$\mathbf{L}_3 = \begin{bmatrix} 0 & -1 & 0 & 0 \\ 1 & 0 & 0 & 0 \\ 0 & 0 & 0 & 0 \\ 0 & 0 & 0 & 0 \end{bmatrix}, \quad \mathbf{L}_6 = \begin{bmatrix} 0 & 0 & 0 & 0 \\ 0 & 0 & 0 & 0 \\ 0 & 0 & 0 & 1 \\ 0 & 0 & 0 & 0 \end{bmatrix}. \quad (3)$$

The Lie algebra is a linear space equipped with a Lie bracket $[\cdot, \cdot] : se(3) \times se(3) \rightarrow se(3)$, which is the product operation in $se(3)$

$$[\mathbf{T}_1, \mathbf{T}_2] = \mathbf{T}_1 \mathbf{T}_2 - \mathbf{T}_2 \mathbf{T}_1 \quad (4)$$

where $\mathbf{T}_1, \mathbf{T}_2 \in se(3)$. Then the *structure constants* of the Lie algebra C_{ij}^k are defined as

$$[\mathbf{L}_i, \mathbf{L}_j] = C_{ij}^k \mathbf{L}_k. \quad (5)$$

Note that an index appears once in the superscript and once in the subscript in a term implies a summation over that index. The summation convention is used throughout this article.

The nonzero structure constants C_{ij}^k are as follows:

$$\begin{aligned} C_{12}^3 &= C_{31}^2 = C_{23}^1 = C_{15}^6 = C_{26}^4 = C_{34}^5 = C_{42}^6 = C_{53}^4 = C_{61}^5 = 1 \\ C_{21}^3 &= C_{13}^2 = C_{32}^1 = C_{51}^6 = C_{62}^4 = C_{43}^5 = C_{24}^6 = C_{35}^4 = C_{16}^5 = -1 \end{aligned} \quad (6)$$

B. Vector Fields

A smooth vector field on the manifold means the tangent vector is attached smoothly at each point. The set of smooth vector fields on $SE(3)$ is denoted as $\mathfrak{X}(SE(3))$.

For any twist $\mathbf{T} \in se(3)$, the *left invariant vector fields* $\hat{\mathbf{T}}$ could be generated by assigning a vector $\hat{\mathbf{T}} \Big|_{\mathbf{A}}$ at every point $\mathbf{A} \in SE(3)$

$$\hat{\mathbf{T}} \Big|_{\mathbf{A}} = \mathbf{A} \mathbf{T}. \quad (7)$$

Using the set of basis $\mathbf{L}_i (i = 1, 2, \dots, 6)$ given above, the basis of left invariant vector fields $\hat{\mathbf{L}}_i (i = 1, 2, \dots, 6)$ are

$$\hat{\mathbf{L}}_i \Big|_{\mathbf{A}} = \mathbf{A} \mathbf{L}_i \quad (i = 1, 2, \dots, 6). \quad (8)$$

The Lie algebra isomorphism lead to

$$[\hat{\mathbf{L}}_i, \hat{\mathbf{L}}_j] = [\widehat{\mathbf{L}_i, \mathbf{L}_j}] = C_{ij}^k \hat{\mathbf{L}}_k. \quad (9)$$

Similarly, the case for the basis of right invariant vector fields are

$$\tilde{\mathbf{L}}_i \Big|_{\mathbf{A}} = \mathbf{L}_i \mathbf{A} \quad (i = 1, 2, \dots, 6) \quad (10)$$

$$[\tilde{\mathbf{L}}_i, \tilde{\mathbf{L}}_j] = -[\widetilde{\mathbf{L}_i, \mathbf{L}_j}] = -C_{ij}^k \tilde{\mathbf{L}}_k. \quad (11)$$

In robotics, we can choose joint variables ξ^i as local coordinates, which generates $\mathbf{E}_i = \frac{\partial}{\partial \xi^i} (i = 1, 2, \dots, n)$. It is called the *coordinate basis*. When n is equal to or less than 6, the joint coordinates can be considered as local coordinates of $SE(3)$ or its submanifold, respectively. The Lie bracket vanishes on the coordinate basis

$$[\mathbf{E}_i, \mathbf{E}_j] = 0. \quad (12)$$

The Jacobian \mathbf{J} represents the velocity relationship between joint and Cartesian space. Here, γ_j^i denotes the i th row and j th column of \mathbf{J} , and α_j^i denotes the i th row and j th column of \mathbf{J}^{-1} (or generalized inverse). When \mathbf{J} is a *body manipulator Jacobian* [52], the following relation holds:

$$\mathbf{E}_i = \gamma_i^j \hat{\mathbf{L}}_j \quad (13a)$$

$$\hat{\mathbf{L}}_i = \alpha_i^j \mathbf{E}_j. \quad (13b)$$

C. Dual Vector Fields

A dual vector field is obtained after a dual vector is given at each point on the manifold. The set of smooth dual vector fields is denoted as $\mathfrak{X}^*(SE(3))$. The dual basis $d\xi^i$ is obtained in the dual space after giving the basis $\frac{\partial}{\partial \xi^i} (i = 1, 2, \dots, n)$. Then, the contraction between the dual and original space is

$$\langle d\xi^i, \mathbf{E}_j \rangle = \delta_j^i \quad (14)$$

where

$$\delta_j^i = \begin{cases} 1 & i = j \\ 0 & i \neq j. \end{cases} \quad (15)$$

D. Other Types of Tensors

A differential k -form on $SE(3)$ is an assignment of an anti-symmetric covariant k th-order tensor to each point. The vector space of smooth k -forms is denoted as $\Omega^k(SE(3))$.

The *Riemann curvature tensor* R can be considered as a measure of how much manifolds deviate from the Euclidean space. For any $X, Y \in \mathfrak{X}(SE(3))$, it can be seen as a mapping $R(X, Y) : \mathfrak{X}(SE(3)) \rightarrow \mathfrak{X}(SE(3))$.

E. Differential Operator

$\nabla_Y X$ is the covariant derivative of X along the direction Y for any $X, Y \in \mathfrak{X}(SE(3))$. After defining the covariant derivative, a rule called *parallel transport* is defined to “connect” the tangent vectors at different points on the manifold. This endows the manifold with a *connection* [51]. If for any $X, Y \in \mathfrak{X}(SE(3))$, a connection always satisfies

$$\nabla_X Y - \nabla_Y X = [X, Y] \quad (16)$$

then the connection is called *symmetric*.

On $SE(3)$ one can define

$$\nabla_{\mathbf{E}_i} \mathbf{E}_j = {}^E \Gamma_{ji}^k \mathbf{E}_k \quad (17a)$$

$$\nabla_{\hat{\mathbf{L}}_i} \hat{\mathbf{L}}_j = {}^L \Gamma_{ji}^k \hat{\mathbf{L}}_k \quad (17b)$$

where ${}^E \Gamma_{ji}^k$ and ${}^L \Gamma_{ji}^k$ are, respectively, the *Christoffel symbols* under basis $\{\mathbf{E}_i\}$ and $\{\hat{\mathbf{L}}_i\}$. By generalizing Leibniz’s law, covariant derivative can be extended to the dual vector fields [48]. For any $U, V \in \mathfrak{X}(SE(3))$, $F \in \mathfrak{X}^*(SE(3))$, the following condition holds:

$$\langle \nabla_U F, V \rangle = U(\langle F, V \rangle) - \langle F, \nabla_U V \rangle. \quad (18)$$

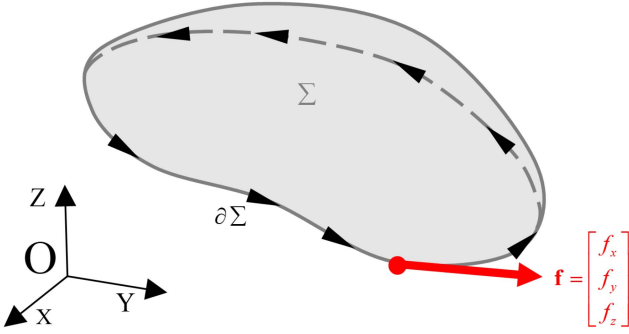


Fig. 2. Conservative system is subjected to the external force \mathbf{f} doing work along a closed path $\partial\Sigma$. Σ is the surface with boundary $\partial\Sigma$.

For the differential forms, there exists *exterior differentiation* $d: \Omega^k(\text{SE}(3)) \rightarrow \Omega^{k+1}(\text{SE}(3))$, satisfying $d \circ d \equiv 0$. For a k -form ω , ω is *exact* if there exists a $(k-1)$ -form η such that $\omega = d\eta$, and *closed* when $d\omega = 0$.

The configuration of a conservative mechanical system determines the potential energy Φ . Then, we get the force one-form $d\Phi$. The torque of i th joint τ_i and the i th component of the wrench \mathcal{F}_i acting on the end-effector are expressed as

$$\tau_i = \langle d\Phi, \mathbf{E}_i \rangle = \frac{\partial \Phi}{\partial \xi^i} \quad (19a)$$

$$\mathcal{F}_i = \langle d\Phi, \hat{\mathbf{L}}_i \rangle = \hat{\mathbf{L}}_i(\Phi). \quad (19b)$$

F. Conservative Stiffness Matrix

In Fig. 2, a conservative system is subjected to a force, and the system translates along a closed path $\partial\Sigma$. When the force \mathbf{f} corresponding to the Cartesian stiffness matrix \mathbf{K} is a point function and the work W done by this force is also a point function, the stiffness matrix is said to be conservative

$$W = \oint_{\partial\Sigma} \mathbf{f} \cdot d\mathbf{x} = 0 \quad (20a)$$

$$\mathbf{f} = \oint_{\partial\Sigma} \mathbf{K} \cdot d\mathbf{x} = \mathbf{0} \quad (20b)$$

where $\mathbf{x} = [x, y, z]^T$.

Kao and Ngo [42] studied the case of translational motion. They transformed the problem into the integration over the surface Σ and pointed out that (20a) and (20b) require the stiffness matrix to be symmetric and exact, respectively:

1) *Symmetry*: $k_{ij} = k_{ji}$ ($1 \leq i, j, k \leq 3$).

2) *Exactness*: $\frac{\partial k_{ij}}{\partial x^k} = \frac{\partial k_{ik}}{\partial x^j}$ ($1 \leq i, j, k \leq 3$).

where k_{ij} means the i th row and j th column of $\mathbf{K} \in \mathbb{R}^{3 \times 3}$.

G. Stiffness Modeling

Howard et al. [39], Žefran and Kumar [44], [53] used differential geometry to study the stiffness matrix. $\nabla_Y d\Phi$ describes the change of force along the vector field Y . The contraction between vector field X and $\nabla_Y d\Phi$ defines the stiffness tensor $K = \nabla d\Phi$ on manifold

$$K(X, Y) = \langle \nabla_Y d\Phi, X \rangle = (YX - \nabla_Y X)(\Phi). \quad (21)$$

Žefran and Kumar [44] showed that a symmetric connection leads to a symmetric stiffness matrix. They stated that the stiffness tensor is symmetric when one of the following conditions is satisfied:

$${}^L\Gamma_{ji}^k - {}^L\Gamma_{ij}^k = C_{ij}^k \quad (22)$$

$${}^E\Gamma_{ij}^k = {}^E\Gamma_{ji}^k. \quad (23)$$

III. CONSERVATIVE STIFFNESS MATRIX ON $T(3)$

From Section II-F, we know that when the mechanical system undergoes translational motion, the simultaneous satisfaction of symmetric and exact conditions guarantees a conservative Cartesian stiffness matrix. The translational motion can be described by the subgroup of $\text{SE}(3)$, which is denoted by $T(3)$. Since symmetry has been studied by many scholars, this section focuses on exactness on $T(3)$.

A. Conservative Stiffness Matrix on $T(3)$

In this section, we give a geometric statement of the conservative stiffness matrix. The following differential forms are constructed based on (20) [x, y , and z are the coordinates on $T(3)$]:

$$\begin{aligned} \omega_0 &= f_x dx + f_y dy + f_z dz, & \omega_1 &= k_{11} dx + k_{12} dy + k_{13} dz \\ \omega_2 &= k_{21} dx + k_{22} dy + k_{23} dz, & \omega_3 &= k_{31} dx + k_{32} dy + k_{33} dz. \end{aligned} \quad (24)$$

When the force and work are point functions in space, it means that the differential forms ω_i ($i = 0, 1, 2, 3$) defined above are exact. Then, the following lemma can be used to solve the above problem.

Lemma 1 (The Poincaré lemma [50]): If B is an open ball in \mathbb{R}^n , any closed k -form defined on B is exact, for any integer k with $1 \leq k \leq n$.

Note that the above ω_i are actually defined in \mathbb{R}^3 . Based on the Poincaré lemma, the closed form is equivalent to the exact form. Therefore, we only need to look for conditions that ensure ω_i ($i = 0, 1, 2, 3$) are closed forms. It is easy to check that

$$d\omega_0 = 0 \Rightarrow k_{ij} = k_{ji}$$

$$d\omega_1 = d\omega_2 = d\omega_3 = 0 \Rightarrow \frac{\partial k_{ij}}{\partial x^k} = \frac{\partial k_{ik}}{\partial x^j}$$

which are exactly the symmetric and exact conditions mentioned before.

It is worth mentioning that the work done as a point function is not guaranteed when the Cartesian stiffness matrix only satisfies the symmetric condition. The satisfaction of the symmetric condition alone does not guarantee that the force is a continuous function in space, which leads to ambiguities in the definition of the stiffness matrix. When the exact condition is further added, both work and force are point functions. This statement will be verified later by numerical simulations in Section VI.

B. Exact Stiffness Matrix on $T(3)$

In this section, the exact Cartesian stiffness matrix is analyzed on $T(3)$. For a conservative mechanical system, the i th row and

j th column of the joint stiffness matrix \mathbf{K}_θ is generally expressed as (here we consider only the most general case, for the case with passive joints and flexible links, see Appendices E and F)

$$[\mathbf{K}_\theta]_{ij} = \mathbf{E}_j \mathbf{E}_i (\Phi) = \frac{\partial^2 \Phi}{\partial \xi_j \partial \xi_i}. \quad (25)$$

In the basis $\{\hat{\mathbf{L}}_i\}$, the components of the stiffness tensor can be expressed as

$$K_{ij}^L = K(\hat{\mathbf{L}}_i, \hat{\mathbf{L}}_j) = (\hat{\mathbf{L}}_j \hat{\mathbf{L}}_i - \nabla_{\hat{\mathbf{L}}_j} \hat{\mathbf{L}}_i)(\Phi). \quad (26)$$

Notice that K_{ij}^L correspond to the components of the Cartesian stiffness matrix, i.e., $K_{ij}^L = [\mathbf{K}_C]_{ij}$.

The condition for the exactness of the Cartesian stiffness matrix on $T(3)$ is

$$\hat{\mathbf{L}}_k (K_{ij}^L) = \hat{\mathbf{L}}_j (K_{ik}^L) \quad (i, j, k = 4, 5, 6). \quad (27)$$

Expand the left side of (27)

$$\begin{aligned} \hat{\mathbf{L}}_k (K_{ij}^L) &= \hat{\mathbf{L}}_k \left((\hat{\mathbf{L}}_j \hat{\mathbf{L}}_i - {}^L \Gamma_{ij}^m \hat{\mathbf{L}}_m) (\Phi) \right) \\ &= \hat{\mathbf{L}}_k \hat{\mathbf{L}}_j \hat{\mathbf{L}}_i (\Phi) - \hat{\mathbf{L}}_k ({}^L \Gamma_{ij}^m \hat{\mathbf{L}}_m (\Phi)) - {}^L \Gamma_{ij}^m \hat{\mathbf{L}}_k \hat{\mathbf{L}}_m (\Phi) \\ &= \frac{\partial^3 \Phi}{\partial x^k \partial x^j \partial x^i} - \frac{\partial {}^L \Gamma_{ij}^m}{\partial x^k} \frac{\partial \Phi}{\partial x^m} - {}^L \Gamma_{ij}^m \frac{\partial^2 \Phi}{\partial x^k \partial x^m}. \end{aligned} \quad (28)$$

Note that exactness implies that (28) is symmetric with respect to the indexes j and k ($i, j, k = 4, 5, 6$). For illustration, a connection that satisfies the exactness condition is called an *exact connection*.

The condition for the exactness (27) can also be written in $\{\mathbf{E}_i\}$. The derivation is more complicated, but we can obtain some new conclusions

$$\begin{aligned} \hat{\mathbf{L}}_k (K_{ij}^L) &= \alpha_k^p \mathbf{E}_p (\alpha_j^l (\mathbf{E}_l \mathbf{E}_m (\Phi) - {}^E \Gamma_{ml}^n \mathbf{E}_n (\Phi)) \alpha_i^m) \\ &= \left(-\alpha_k^l \alpha_j^p \alpha_i^m {}^E \Gamma_{np}^m + \alpha_k^p \frac{\partial (\alpha_j^l \alpha_i^m)}{\partial \xi^p} \right) \frac{\partial^2 \Phi}{\partial \xi^l \partial \xi^m} \\ &\quad + \alpha_k^p \alpha_j^l \alpha_i^m \frac{\partial^3 \Phi}{\partial \xi^p \partial \xi^l \partial \xi^m} - \alpha_k^p \frac{\partial (\alpha_j^l {}^E \Gamma_{ml}^n \alpha_i^m)}{\partial \xi^p} \frac{\partial \Phi}{\partial \xi^n}. \end{aligned} \quad (29)$$

To see more clearly the relationship between joint and Cartesian stiffness matrix, the above equation is expressed as

$$\begin{aligned} \hat{\mathbf{L}}_k (K_{ij}^L) &= \left(-\alpha_k^l \alpha_j^p \alpha_i^m {}^E \Gamma_{np}^m + \alpha_k^p \frac{\partial (\alpha_j^l \alpha_i^m)}{\partial \xi^p} \right) [\mathbf{K}_\theta]_{ml} \\ &\quad + \alpha_k^p \alpha_j^l \alpha_i^m \frac{\partial [\mathbf{K}_\theta]_{ml}}{\partial \xi^p} - \alpha_k^p \frac{\partial (\alpha_j^l {}^E \Gamma_{ml}^n \alpha_i^m)}{\partial \xi^p} \tau_n \\ &= [\mathbf{C}_1]_{kji}^{lm} [\mathbf{K}_\theta]_{ml} + [\mathbf{C}_2]_{kji}^{plm} \frac{\partial [\mathbf{K}_\theta]_{ml}}{\partial \xi^p} + [\mathbf{C}_3]_{kji}^n \tau_n \end{aligned} \quad (30)$$

exactness implies that (30) is symmetric with respect to the indexes j and k which means the following condition:

$$[\mathbf{C}_1]_{kji}^{lm} = [\mathbf{C}_1]_{jki}^{lm} \quad (31a)$$

$$\frac{\partial [\mathbf{K}_\theta]_{ml}}{\partial \xi^p} = \frac{\partial [\mathbf{K}_\theta]_{mp}}{\partial \xi^l} \quad (31b)$$

$$[\mathbf{C}_3]_{kji}^n = [\mathbf{C}_3]_{jki}^n \quad (31c)$$

where (31b) means the exactness of the joint stiffness matrix.

According to (30), the following corollaries for the stiffness matrix on $T(3)$ could be concluded.

Corollary 1: If the joint stiffness matrix is not exact, the Cartesian stiffness matrix will not be exact either. The indexes asymmetry of the $[\mathbf{C}_2]_{kji}^{plm} \frac{\partial [\mathbf{K}_\theta]_{ml}}{\partial \xi^p}$ term will generally result in overall asymmetry of (30).

Corollary 2: When the joint stiffness matrix is exact but asymmetric, the resulting Cartesian stiffness matrix could still be exact. In fact, the asymmetric and exact joint stiffness matrix generates an asymmetric and exact Cartesian stiffness matrix by CCT on $T(3)$. The complete proof procedure is shown in Appendix A.

Corollary 3: The exact condition (31a) can be relaxed when the joint stiffness matrix is symmetric: $[\mathbf{C}_1]_{kji}^{lm} + [\mathbf{C}_1]_{kji}^{ml}$ are symmetric with respect to indexes j and k .

IV. PROPERTY OF CARTESIAN STIFFNESS MATRIX UNDER CCT

Salisbury [17] and Gosselin [18] proposed the conventional stiffness mapping between \mathbf{K}_θ and \mathbf{K}_c . Then, Chen and Kao [21] derived the CCT. In this section, the geometric implication of CCT is explained, and further, the properties of the Cartesian stiffness matrix under CCT on $T(3)$ and $SE(3)$ are given.

A. Connection Corresponding to CCT

In contrast to the conventional stiffness mapping, $\mathbf{K}_C = \mathbf{J}^{-T} \mathbf{K}_\theta \mathbf{J}^{-1}$, the CCT stiffness mapping

$$\mathbf{K}_C = \mathbf{J}^{-T} (\mathbf{K}_\theta - \mathbf{K}_g) \mathbf{J}^{-1} \quad (32)$$

where the matrix \mathbf{K}_g is written as $\left[\left(\frac{\partial \mathbf{J}^T}{\partial \xi^T} \mathcal{F} \right) \left(\frac{\partial \mathbf{J}^T}{\partial \xi^2} \mathcal{F} \right) \dots \left(\frac{\partial \mathbf{J}^T}{\partial \xi^n} \mathcal{F} \right) \right]$, introduces term \mathbf{K}_g describing the Jacobi variation and external loads. $\mathcal{F} = [\mathbf{m}^T \quad \mathbf{f}^T]^T$ is the wrench applied at the end-effector, where \mathbf{m} is the moment. The component representation of (32) is

$$\begin{aligned} [\mathbf{K}_C]_{ij} &= \alpha_i^k [\mathbf{K}_\theta]_{kl} \alpha_j^l - \alpha_i^k \frac{\partial \gamma_k^p}{\partial \xi^l} \mathcal{F}_p \alpha_j^l \\ &= \alpha_i^k [\mathbf{K}_\theta]_{kl} \alpha_j^l - \alpha_i^k \frac{\partial \gamma_k^p}{\partial \xi^l} \alpha_p^m \mathbf{E}_m (\Phi) \alpha_j^l \end{aligned} \quad (33)$$

where $\mathcal{F}_p = \hat{\mathbf{L}}_p (\Phi) = \alpha_p^m \mathbf{E}_m (\Phi)$.

Notice that

$$\begin{aligned} K_{ij}^L &= \left\langle \nabla_{\alpha_j^l \mathbf{E}_l} d\Phi, \alpha_i^k \mathbf{E}_k \right\rangle \\ &= \alpha_i^k (\mathbf{E}_l \mathbf{E}_k - \nabla_{\mathbf{E}_l} \mathbf{E}_k) (\Phi) \alpha_j^l \\ &= \alpha_i^k \mathbf{E}_l \mathbf{E}_k (\Phi) \alpha_j^l - \alpha_i^k {}^E \Gamma_{kl}^m \mathbf{E}_m (\Phi) \alpha_j^l. \end{aligned} \quad (34)$$

According to the work of Howard et al. [39] and the physical meaning

$$[\mathbf{K}_C]_{ij} = K_{ij}^L, [\mathbf{K}_\theta]_{kl} = \mathbf{E}_l \mathbf{E}_k (\Phi).$$

Comparing (33) and (34), the connection corresponding to CCT is given

$$E\Gamma_{kl}^m = \frac{\partial \gamma_k^p}{\partial \xi^l} \alpha_p^m. \quad (35)$$

By definition $\alpha_p^m \gamma_k^p = \delta_k^m$, one can get

$$E\Gamma_{kl}^m = \frac{\partial \gamma_k^p}{\partial \xi^l} \alpha_p^m = -\frac{\partial \alpha_p^m}{\partial \xi^l} \gamma_k^p. \quad (36)$$

Then, the Christoffel symbols under basis $\{\hat{\mathbf{L}}_i\}$ could be calculated

$$\begin{aligned} \nabla_{\hat{\mathbf{L}}_j} \hat{\mathbf{L}}_i &= \nabla_{\alpha_j^l \mathbf{E}_l} \alpha_i^k \mathbf{E}_k \\ &= \alpha_j^l \mathbf{E}_l (\alpha_i^k) \mathbf{E}_k + \alpha_j^l \alpha_i^k \nabla_{\mathbf{E}_l} \mathbf{E}_k \\ &= \alpha_j^l \left(\frac{\partial \alpha_i^k}{\partial \xi^l} \gamma_k^m + \alpha_i^k \frac{\partial \gamma_k^m}{\partial \xi^l} \right) \hat{\mathbf{L}}_m \\ &= \alpha_j^l \frac{\partial \delta_i^m}{\partial \xi^l} \hat{\mathbf{L}}_m \\ &= 0. \end{aligned} \quad (37)$$

The result in (37) means that ${}^L\Gamma_{ij}^m \equiv 0$ under the basis $\{\hat{\mathbf{L}}_i\}$. Then, the components of Cartesian stiffness matrix can be written as

$$K_{ij}^L = \hat{\mathbf{L}}_j \hat{\mathbf{L}}_i (\Phi). \quad (38)$$

This is the same as the stiffness matrix defined in [35], [36], [39], [46].

Proposition 1: The stiffness transformation (32) has the same geometric connotation as the stiffness matrix defined in [35], [36], [39], [46].

Proposition 2: The CCT corresponds to a flat connection in basis $\{\hat{\mathbf{L}}_i\}$, while the conventional stiffness transformation corresponds to a flat connection in basis $\{\mathbf{E}_i\}$.

Proof: When the connection is flat under basis $\{\mathbf{E}_i\}$, i.e., $\nabla_{\mathbf{E}_l} \mathbf{E}_k = 0$:

$$\begin{aligned} K_{ij}^L &= \alpha_i^k (\mathbf{E}_l \mathbf{E}_k - \nabla_{\mathbf{E}_l} \mathbf{E}_k) (\Phi) \alpha_j^l \\ &= \alpha_i^k \frac{\partial^2 \Phi}{\partial \xi^l \partial \xi^k} \alpha_j^l. \end{aligned} \quad (39)$$

The above equation is expressed in matrix form, which just corresponds to the conventional stiffness transformation $\mathbf{K}_C = \mathbf{J}^{-T} \mathbf{K}_\theta \mathbf{J}^{-1}$. \square

Notice that in this section, we default $[\mathbf{K}_\theta]_{ij} = \mathbf{E}_j \mathbf{E}_i (\Phi)$, so in the next Sections IV-B and IV-C, we discuss the properties of the Cartesian stiffness matrix on the assumption that \mathbf{K}_θ is symmetric and exact.

B. Property on $T(3)$

On $T(3)$, note that all of the structure constants vanish

$$C_{45}^k = C_{46}^k = C_{56}^k = C_{54}^k = C_{64}^k = C_{65}^k = 0. \quad (k=1, 2, \dots, 6). \quad (40)$$

This implies that the symmetric condition for Cartesian stiffness matrix on $T(3)$ would be satisfied

$${}^L\Gamma_{ji}^k - {}^L\Gamma_{ij}^k = 0 = C_{ij}^k. \quad (41)$$

When ${}^L\Gamma_{ij}^m \equiv 0$, the exactness equation becomes as follows:

$$\begin{aligned} \hat{\mathbf{L}}_k (K_{ij}^L) &= \frac{\partial^3 \Phi}{\partial x^k \partial x^j \partial x^i} - \frac{\partial {}^L\Gamma_{ij}^m}{\partial x^k} \frac{\partial \Phi}{\partial x^m} - {}^L\Gamma_{ij}^m \frac{\partial^2 \Phi}{\partial x^k \partial x^m} \\ &= \frac{\partial^3 \Phi}{\partial x^k \partial x^j \partial x^i}. \end{aligned} \quad (42)$$

The derivatives of Φ with respect to the coordinate basis $\frac{\partial}{\partial x^i}$ ($i=4, 5, 6$) are exchangeable. So, $\hat{\mathbf{L}}_k (K_{ij}^L)$ is symmetric with respect to indexes j and k which means that the Cartesian stiffness matrix is exact on $T(3)$.

In summary, the stiffness matrix under CCT is conservative on $T(3)$.

Combining the above discussion with Corollary 2, we obtain the following corollary.

Corollary 4: The exact and symmetric joint stiffness matrix \mathbf{K}_θ corresponds to the conservative Cartesian stiffness matrix \mathbf{K}_C under CCT on $T(3)$.

C. The Property on $SE(3)$

Now coming to the more general case, consider the 6-D rigid body motion. Since the structure constants do not vanish, the symmetric condition is no longer satisfied

$${}^L\Gamma_{ji}^k - {}^L\Gamma_{ij}^k = 0 \neq C_{ij}^k. \quad (43)$$

It is easy to calculate the skew-symmetric matrix \mathbf{K}_{skew}

$$\begin{aligned} [\mathbf{K}_{skew}]_{ij} &= \frac{[\mathbf{K}_C]_{ij} - [\mathbf{K}_C]_{ji}}{2} \\ &= \frac{1}{2} (\hat{\mathbf{L}}_j \hat{\mathbf{L}}_i - \hat{\mathbf{L}}_i \hat{\mathbf{L}}_j) (\Phi) = -\frac{1}{2} [\hat{\mathbf{L}}_i, \hat{\mathbf{L}}_j] (\Phi) \\ &= -\frac{1}{2} [\widehat{\mathbf{L}_i, \mathbf{L}_j}] (\Phi) = -\frac{1}{2} C_{ij}^k \hat{\mathbf{L}}_k (\Phi) \\ &= -\frac{1}{2} C_{ij}^k \mathcal{F}_k \end{aligned} \quad (44)$$

where \mathcal{F}_k is the k th component of the wrench in body frame. The above equation can be expressed as the following matrix expression:

$$\mathbf{K}_{skew} = \frac{1}{2} \begin{bmatrix} [\mathbf{m}] & [\mathbf{f}] \\ [\mathbf{f}] & \mathbf{0} \end{bmatrix} \quad (45)$$

where

$$\begin{aligned} [\mathbf{m}] &= \begin{bmatrix} 0 & -\mathcal{F}_3 & \mathcal{F}_2 \\ \mathcal{F}_3 & 0 & -\mathcal{F}_1 \\ -\mathcal{F}_2 & \mathcal{F}_1 & 0 \end{bmatrix}, \\ [\mathbf{f}] &= \begin{bmatrix} 0 & -\mathcal{F}_6 & \mathcal{F}_5 \\ \mathcal{F}_6 & 0 & -\mathcal{F}_4 \\ -\mathcal{F}_5 & \mathcal{F}_4 & 0 \end{bmatrix}. \end{aligned} \quad (46)$$

Notice that the Jacobian matrix is the spatial manipulator Jacobian and the twist is the spatial velocity [52] when using

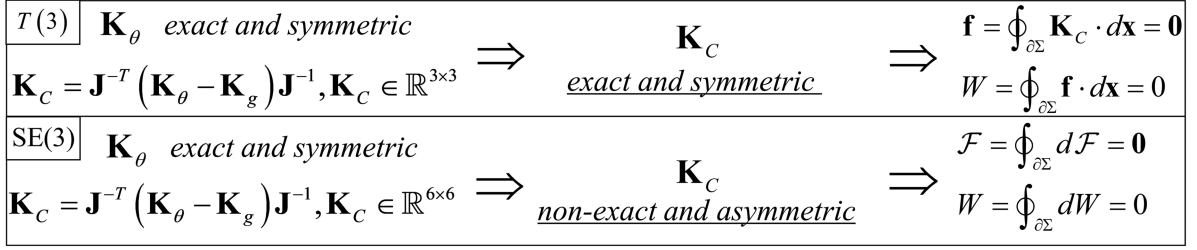


Fig. 3. Schematic diagram of the conservative Cartesian stiffness matrix \mathbf{K}_C on $T(3)$ and $SE(3)$. An exact and symmetric \mathbf{K}_θ always generates a conservative \mathbf{K}_C under CCT. This also illustrates that a Cartesian stiffness matrix \mathbf{K}_C can still be conservative when it is not symmetric and exact on $SE(3)$.

the right invariant vector fields. In this case, \mathbf{K}_{skew} could be written as

$$\begin{aligned} [\mathbf{K}_{\text{skew}}]_{ij} &= -\frac{1}{2} [\tilde{\mathbf{L}}_i, \tilde{\mathbf{L}}_j] (\Phi) \\ &= \frac{1}{2} [\widetilde{[\mathbf{L}_i, \mathbf{L}_j]}] (\Phi) = \frac{1}{2} C_{ij}^k \tilde{\mathbf{L}}_k (\Phi) \\ &= \frac{1}{2} C_{ij}^k \bar{\mathcal{F}}_k \end{aligned} \quad (47)$$

where $\bar{\mathcal{F}}_k$ is the k th component of the wrench in spatial frame. The same results are presented in [36], [43], [46], but here we obtained this conclusion with a more concise and geometric perspective.

It is easy to check that $\alpha_k^p \frac{\partial \alpha_j^l}{\partial \xi^p}$ is generally not symmetric about the indicators j and k on $SE(3)$, i.e.,

$$\alpha_k^p \frac{\partial \alpha_j^l}{\partial \xi^p} \neq \alpha_j^p \frac{\partial \alpha_k^l}{\partial \xi^p}. \quad (48)$$

Combining (95), we obtain that the exact condition on $SE(3)$ does not hold

$$\hat{\mathbf{L}}_k (K_{ij}^L) \neq \hat{\mathbf{L}}_j (K_{ik}^L) \cdot (i, j, k = 1, 2, \dots, 6) \quad (49)$$

Although the Cartesian stiffness matrix \mathbf{K}_C under CCT on $SE(3)$ is neither symmetric nor exact, it still has the following mechanical properties.

Proposition 3: For an arbitrary \mathbf{K}_θ , the work done by joint torque is constantly equal to the work done by the end external wrench under CCT. See Appendix B for details.

Proposition 4: The exact and symmetric joint stiffness matrix \mathbf{K}_θ corresponds to the conservative Cartesian stiffness matrix \mathbf{K}_C under CCT on $SE(3)$. See Appendix C for details.

Comparing Corollary 4 and Proposition 4, we find that a symmetric and exact \mathbf{K}_θ always corresponds to the conservative \mathbf{K}_C , either on $T(3)$ or $SE(3)$, as shown in Fig. 3. This is consistent with the physical intuition i.e., a conservative \mathbf{K}_θ corresponds to a conservative \mathbf{K}_C . This has important implications for the design of control law for actual robotic systems (see Section VII-B).

V. OTHER CONNECTIONS AND STIFFNESS MAPPING

In this section, the connections that satisfy the symmetric or exact conditions on $T(3)$ are solved. We then give a one-to-one correspondence between the connection and the stiffness mapping on the manifold.

In Sections V-A, V-B, and V-C, $[\mathbf{K}_\theta]_{ij} = \mathbf{E}_j \mathbf{E}_i (\Phi)$, so in these sections we default \mathbf{K}_θ is symmetric and exact.

A. Symmetric Connection on $T(3)$

As mentioned before, all of the symmetric connections have to be constrained by the equation ${}^E \Gamma_{ij}^k = {}^E \Gamma_{ji}^k$.

From (34) the relationship between joint and Cartesian stiffness matrix is obtained

$$[\mathbf{K}_C]_{ij} = \alpha_i^k [\mathbf{K}_\theta]_{kl} \alpha_j^l - \alpha_i^k {}^E \Gamma_{kl}^m \mathbf{E}_m (\Phi) \alpha_j^l. \quad (50)$$

When substituting the symmetric connections into (50) and organizing the component expressions into matrices, the following stiffness mapping equation is obtained:

$$\mathbf{K}_C = \mathbf{J}^{-T} (\mathbf{K}_\theta + \mathbf{S}) \mathbf{J}^{-1} \quad (51)$$

where \mathbf{S} is a symmetric matrix, i.e., $\mathbf{S} = \mathbf{S}^T$.

B. Exact Connection on $T(3)$

A connection satisfies the exact condition on $T(3)$ means the equation below is symmetric with respect to the indexes j and k

$$\hat{\mathbf{L}}_k (K_{ij}^L) = \frac{\partial^3 \Phi}{\partial x^k \partial x^j \partial x^i} - \frac{\partial^L \Gamma_{ij}^m}{\partial x^k} \frac{\partial \Phi}{\partial x^m} - L \Gamma_{ij}^m \frac{\partial^2 \Phi}{\partial x^k \partial x^m}. \quad (52)$$

Since the potential energy function Φ is chosen arbitrarily, the index symmetry implies that the following equation holds:

$$\frac{\partial^L \Gamma_{ij}^m}{\partial x^k} = \frac{\partial^L \Gamma_{ik}^m}{\partial x^j} \quad (53a)$$

$$L \Gamma_{ij}^m \frac{\partial^2 \Phi}{\partial x^k \partial x^m} = L \Gamma_{ik}^m \frac{\partial^2 \Phi}{\partial x^j \partial x^m}. \quad (53b)$$

In order for (53b) to hold, the following equations must be satisfied:

$$L \Gamma_{i4}^4 = L \Gamma_{i5}^5 = L \Gamma_{i6}^6 \quad (i = 4, 5, 6) \quad (54a)$$

$$L \Gamma_{ij}^k = 0 \quad (j \neq k, 4 \leq i, j, k \leq 6). \quad (54b)$$

When $m = k \neq j$ and considering (54), (53a) becomes

$$\frac{\partial^L \Gamma_{ij}^m}{\partial x^k} = 0 = \frac{\partial^L \Gamma_{ik}^k}{\partial x^j} = \frac{\partial^L \Gamma_{ij}^j}{\partial x^j}. \quad (55)$$

This means $L \Gamma_{ij}^j$ is constant on $T(3)$.

TABLE II
 STIFFNESS MAPPING ON $T(3)$ ¹

| Connection | Stiffness Mapping | The Properties of \mathbf{K}_C ² |
|---|---|---|
| ${}^E\Gamma_{ij}^m \equiv 0$ | $\mathbf{K}_C = \mathbf{J}^{-T} \mathbf{K}_\theta \mathbf{J}^{-1}$ (CT) [17], [18] | Symmetric |
| ${}^L\Gamma_{ij}^m \equiv 0$ | $\mathbf{K}_C = \mathbf{J}^{-T} (\mathbf{K}_\theta - \mathbf{K}_g) \mathbf{J}^{-1}$ (CCT) [21] | Conservative (Symmetric and Exact) |
| ${}^E\Gamma_{ij}^k = {}^E\Gamma_{ji}^k$ | $\mathbf{K}_C = \mathbf{J}^{-T} (\mathbf{K}_\theta + \mathbf{S}) \mathbf{J}^{-1}$ | Symmetric |
| ${}^L\Gamma_{i4}^4 = {}^L\Gamma_{i5}^5 = {}^L\Gamma_{i6}^6 = \text{constant}$ | $\mathbf{K}_C = \mathbf{J}^{-T} (\mathbf{K}_\theta - \mathbf{K}_g - \mathbf{J}^T \mathbf{c} \boldsymbol{\tau}^T) \mathbf{J}^{-1}$ (ECT) | Exact |
| ${}^L\Gamma_{ij}^k = 0$ ($j \neq k, 4 \leq i, j, k \leq 6$) | | |

¹ $\mathbf{K}_C = \mathbf{J}^{-T} (\mathbf{K}_\theta + \mathbf{S}) \mathbf{J}^{-1}$ is the general solution that produces a symmetric Cartesian stiffness matrix. When $\mathbf{S} = \mathbf{0}$, the mapping degenerates to CT. ECT is the general solution that produces an exact Cartesian stiffness matrix on $T(3)$. When $\mathbf{c} = \mathbf{0}$, the mapping degenerates to CCT.

² The properties of \mathbf{K}_C are based on the precondition that \mathbf{K}_θ is symmetric and exact.

Then, the solution of (53) is as follows:

$${}^L\Gamma_{i4}^4 = {}^L\Gamma_{i5}^5 = {}^L\Gamma_{i6}^6 = \text{constant} \quad (i = 4, 5, 6) \quad (56a)$$

$${}^L\Gamma_{ij}^k = 0 \quad (j \neq k, 4 \leq i, j, k \leq 6). \quad (56b)$$

Similarly, combining (50) and (56), the corresponding stiffness mapping relationship is obtained

$$\mathbf{K}_C = \mathbf{J}^{-T} (\mathbf{K}_\theta - \mathbf{K}_g - \mathbf{J}^T \mathbf{c} \boldsymbol{\tau}^T) \mathbf{J}^{-1} \quad (57)$$

which could be called the exact congruence transformation (ECT).

When the principle of virtual work holds, (57) can be expressed as follows:

$$\mathbf{K}_C = \mathbf{J}^{-T} (\mathbf{K}_\theta - \mathbf{K}_g) \mathbf{J}^{-1} - \mathbf{c} \boldsymbol{\mathcal{F}}^T \quad (58)$$

where $\mathbf{c} = [c_1 \ c_2 \ c_3]^T$, $c_i = \text{constant}$.

Although ECT is derived from $T(3)$, it still has the following properties on $\text{SE}(3)$.

Proposition 5: On $\text{SE}(3)$, the exact and symmetric joint stiffness matrix \mathbf{K}_θ generates the Cartesian stiffness matrix \mathbf{K}_C such that the wrench $\boldsymbol{\mathcal{F}}$ is a point function under ECT, i.e., $\boldsymbol{\mathcal{F}} = \oint_{\partial\Sigma} d\boldsymbol{\mathcal{F}} = \mathbf{0}$. See Appendix D for details.

C. Conservative Connection on $T(3)$

For illustration, the connection satisfying symmetric and exact conditions is said to be *conservative*. Combining the symmetric condition (22) and the exact condition (56) leads to the following solution:

$${}^L\Gamma_{ij}^k = 0 \quad (4 \leq i, j, k \leq 6) \quad (59)$$

which is exactly the connection corresponding to CCT. This means that the connection corresponding to CCT is the only conservative connection on $T(3)$.

At this point, the stiffness mapping is exactly the CCT (32).

D. Stiffness Mapping on Manifold

The connection determines the stiffness mapping. Conventional stiffness mapping is firstly considered. In this case: ${}^E\Gamma_{ij}^m \equiv 0$, and the Riemann curvature tensor has vanished components under coordinate basis $\{\mathbf{E}_i\}$: $R(\mathbf{E}_i, \mathbf{E}_j)\mathbf{E}_k = 0$, which means a “flat” joint space in the sense of the Riemann curvature tensor.

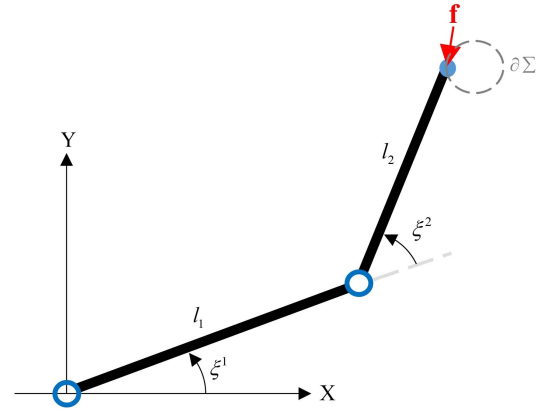


Fig. 4. Illustration of the two-link manipulator. The end-effector moves along the closed path $\partial\Sigma$ and at each moment the elastic force of the system is in equilibrium with the external force \mathbf{f} .

When it comes to CCT case, ${}^L\Gamma_{ij}^m \equiv 0$, and the Riemann curvature tensor has vanished components under $\{\hat{\mathbf{L}}_i\}$: $R(\hat{\mathbf{L}}_i, \hat{\mathbf{L}}_j)\hat{\mathbf{L}}_k = 0$, which means a “flat” end-operation space in the sense of the Riemann curvature tensor.

Remark 1: Different connections lead to different stiffness mappings. See Tables II and III for details.

VI. NUMERICAL SIMULATION OF STIFFNESS MAPPING

In this section, numerical simulations are conducted to investigate the properties of the Cartesian stiffness matrix for different stiffness mappings and joint stiffness matrices. To illustrate the generality of the conclusions, simulations were performed for different types of manipulators. The joint-based control strategy will be used, i.e., \mathbf{K}_c is obtained by stiffness mapping based on the given \mathbf{K}_θ .

A. Case 1: Two-Link Manipulator

The first case is the two-link manipulator in Fig. 4. The end-effector moves along a closed path under the action of \mathbf{f} . The external force \mathbf{f} is considered to be in balance with the elastic force of the system. During this process, the joint torque, as well as the external force, continuously changes and produces work along the path $\partial\Sigma$.

In this simulation, the length of links are $l_1 = 0.29$ m, $l_2 = 0.23$ m. The joint torque is $\boldsymbol{\tau}_0 = [10 \ 20]^T \text{N} \cdot \text{m}$ at the initial

TABLE III
STIFFNESS TENSOR $K = \nabla d\Phi$ ON $SE(3)^1$

| Connection | Model and Assumptions | Stiffness Mapping |
|---------------------------|---|--|
| $E\Gamma_{ij}^m \equiv 0$ | Serial or parallel manipulator | $\mathbf{K}_C = \mathbf{J}^{-T} \mathbf{K}_\theta \mathbf{J}^{-1}$ [17], [18] |
| $E\Gamma_{ij}^m \equiv 0$ | Serial or parallel manipulator with passive joints and flexible links | $\begin{bmatrix} \mathbf{K}_C & * \\ * & * \end{bmatrix} = \begin{bmatrix} \mathbf{J}_\theta \mathbf{K}_\theta^{-1} \mathbf{J}_\theta^T & \mathbf{J}_q \\ \mathbf{J}_q^T & \mathbf{0} \end{bmatrix}^{-1}$ [12] |
| $L\Gamma_{ij}^m \equiv 0$ | Serial or parallel manipulator with external load | $\mathbf{K}_C = \mathbf{J}^{-T} (\mathbf{K}_\theta - \mathbf{K}_g) \mathbf{J}^{-1}$ [21] |
| $L\Gamma_{ij}^m \equiv 0$ | Parallel manipulator with external load and elastic passive joints | $\mathbf{K}_C = \mathbf{J}^{-T} (\mathbf{K}_\theta - \mathbf{K}_g + \mathbf{K}_I) \mathbf{J}^{-1}$ [24] |
| $L\Gamma_{ij}^m \equiv 0$ | Serial or parallel manipulator with external load, passive joints and flexible links | $\begin{bmatrix} \mathbf{K}_C & * & * \\ * & * & * \\ * & * & * \end{bmatrix} = \begin{bmatrix} \mathbf{0} & \mathbf{J}_q & \mathbf{J}_\theta \\ \mathbf{J}_q^T & \mathbf{H}_{qq}^{\mathcal{F}} & \mathbf{H}_{q\theta}^{\mathcal{F}} \\ \mathbf{J}_\theta^T & \mathbf{H}_{\theta q}^{\mathcal{F}} & \mathbf{H}_{\theta\theta}^{\mathcal{F}} - \mathbf{K}_\theta \end{bmatrix}^{-1}$ [13] |
| $L\Gamma_{ij}^m \equiv 0$ | Serial or parallel manipulator with internal and external load, passive joints and flexible links | $\begin{bmatrix} \mathbf{K}_C & * & * \\ * & * & * \\ * & * & * \end{bmatrix} = \begin{bmatrix} \mathbf{0} & \mathbf{J}_q & \mathbf{J}_\theta \\ \mathbf{J}_q^T & \mathbf{H}_{qq} & \mathbf{H}_{q\theta} \\ \mathbf{J}_\theta^T & \mathbf{H}_{\theta q} & \mathbf{H}_{\theta\theta} - \mathbf{K}_\theta \end{bmatrix}^{-1}$ [16] |

¹ The work of other scholars can be unified into the geometric framework. Although different mechanical assumptions correspond to different stiffness models, these models can all be described by the stiffness tensor $K = \nabla d\Phi$. The derivation of the above equations is shown in Appendix E and F.

moment, and the initial external force can be calculated according to the principle of virtual work $\mathbf{f}_0 = (\mathbf{J}^T)^{-1} \boldsymbol{\tau}_0$. To express physical quantities in spatial frame, the spatial manipulator Jacobian is used. The initial joint angle is $\boldsymbol{\xi}_0 = [1.21 \quad -1.09]^T$ rad. The motion path is a circle, and the circle $\mathbf{r}(t)$ can be expressed as follows (Unit: m):

$$\mathbf{r}(t) = \begin{bmatrix} 0.25 \\ 0.30 \end{bmatrix} + 0.08 \begin{bmatrix} \cos \alpha(t) \\ \sin \alpha(t) \end{bmatrix}, \alpha(t) \in [0, 2\pi]. \quad (60)$$

For demonstration, the conventional stiffness mapping, $\mathbf{K}_C = \mathbf{J}^{-T} \mathbf{K}_\theta \mathbf{J}^{-1}$, is denoted as conventional transformation (CT). $\mathbf{K}_C = \mathbf{J}^{-T} (\mathbf{K}_\theta - \mathbf{K}_g) \mathbf{J}^{-1}$ is denoted as CCT. $\mathbf{K}_C = \mathbf{J}^{-T} (\mathbf{K}_\theta - \mathbf{K}_g - \mathbf{J}^T \mathbf{c} \boldsymbol{\tau}^T) \mathbf{J}^{-1}$ is denoted as ECT.

In the simulation, various \mathbf{K}_θ with different properties are considered: symmetric and exact (constant) matrix \mathbf{K}_1 , asymmetric and exact (constant) matrix \mathbf{K}_2 , symmetric and exact (nonconstant) matrix \mathbf{K}_3 , symmetric and nonexact (nonconstant) matrix \mathbf{K}_4 . They are expressed separately as follows (Unit: $\text{N} \cdot \text{m}/\text{rad}$):

$$\mathbf{K}_1 = \text{diag}(10, 20) \quad (61)$$

$$\mathbf{K}_2 = \begin{bmatrix} 10 & 0 \\ 10 & 20 \end{bmatrix} \quad (62)$$

$$\mathbf{K}_3 = \text{diag}(10 \sin \xi^1, 20 \cos \xi^2) \quad (63)$$

$$\mathbf{K}_4 = \text{diag}(10 \sin \xi^2, 20 \cos \xi^1). \quad (64)$$

There are also different parameter selections for \mathbf{c} when it comes to ECT. When $\mathbf{c} = \mathbf{0}$, the stiffness mapping degenerates to the CCT. As \mathbf{c} deviates from the zero value, a more asymmetric Cartesian stiffness matrix is generated in general. The selected parameters in this simulation are as follows:

$$\mathbf{c}_1 = [5 \quad 10]^T \quad (65)$$

$$\mathbf{c}_2 = [10 \quad 20]^T \quad (66)$$

$$\mathbf{c}_3 = [15 \quad 30]^T. \quad (67)$$

The direction of \mathbf{c}_1 to \mathbf{c}_3 is kept constant and the magnitude gradually becomes larger to explore the relationship between symmetry and work done by external forces.

Using the values of the Cartesian and joint stiffness matrix in each configuration, the calculation of forces and work is performed in joint space as well as in Cartesian space, respectively, by combining numerical integration methods. The trapezoidal integral is selected here for numerical simulation

$$\mathbf{f}(t) = \mathbf{f}(t-1) + \mathbf{K}_C d\mathbf{x} \quad (68a)$$

$$W(t) = W(t-1) + \mathbf{f}(t)^T d\mathbf{x} + \frac{1}{2} d\mathbf{x}^T \mathbf{K}_C d\mathbf{x} \quad (68b)$$

$$\boldsymbol{\tau}(t) = \boldsymbol{\tau}(t-1) + \mathbf{K}_\theta d\boldsymbol{\xi} \quad (68c)$$

$$W(t) = W(t-1) + \boldsymbol{\tau}(t)^T d\boldsymbol{\xi} + \frac{1}{2} d\boldsymbol{\xi}^T \mathbf{K}_\theta d\boldsymbol{\xi}. \quad (68d)$$

The simulation of the two-link manipulator is shown in Fig. 5. In Fig. 5(a) and (b), the parameter angle $\alpha(t)$ changes from 0 to 2π (7200 simulation steps), which means that the end-effector performs a closure path. The degree is used as the angle unit in the figures for clarity. The Cartesian stiffness matrix obtained under different stiffness mappings is further integrated to obtain the external loads. For illustration, only the component of the external force f_x in the X direction is shown in Fig. 5(a). All other force components exhibit similar patterns.

Some observations about Fig. 5 are as follows:

- 1) In Fig. 5(b), the symmetric \mathbf{K}_1 produces a symmetric but nonexact Cartesian stiffness matrix through CT, and the net work done by the external force on the closed path is not zero. In contrast, \mathbf{K}_1 produces a symmetric and exact Cartesian stiffness matrix through CCT, in which case the net work done by the external force is zero. It means that the symmetry of the Cartesian stiffness matrix is not a sufficient condition for the net work along the closed path to be zero, and when the exactness condition is further added, the net work done on the closed path is zero. The simulation result is consistent with the statement in Section III-A.
- 2) \mathbf{K}_2 combined with CCT or \mathbf{K}_1 combined with ECT both produce exact but asymmetric Cartesian stiffness matrices.

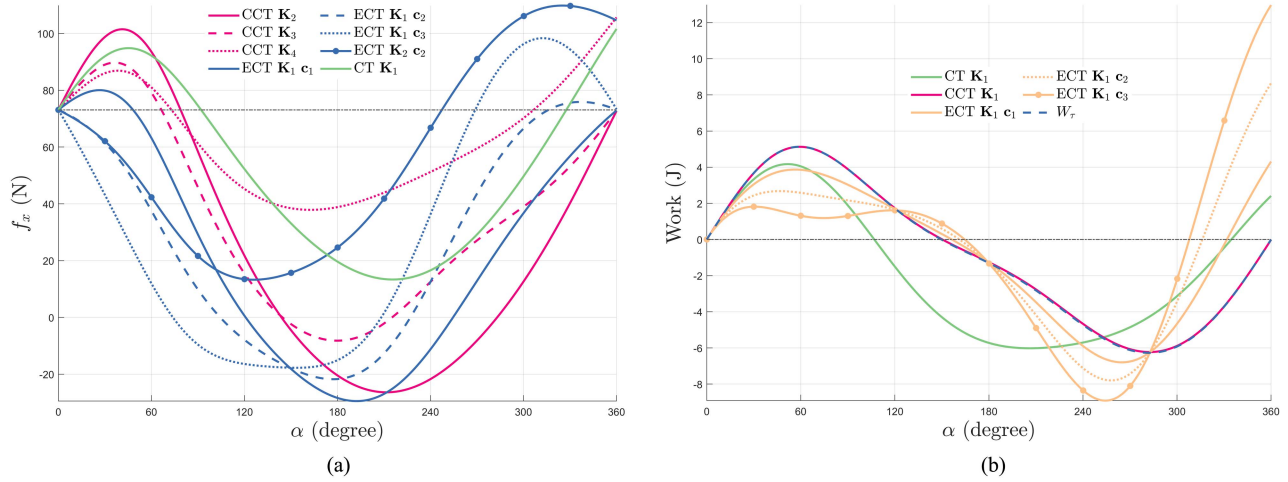


Fig. 5. Simulation of two-link manipulator case for the joint-based control strategy: The specific parameter descriptions are given in Section VI-A. The left and right diagrams show the trend of external force and work done when the end-effector executes the complete closed path respectively. (a) Force curves for different stiffness mappings and different parameters. (b) Work curves for different stiffness mappings and different parameters. The blue dashed line indicates the work done in joint space, and the other lines indicate the work done in Cartesian space.

In Fig. 5(a), the forces are point functions in all these cases. This illustrates that when the Cartesian stiffness matrix is exact and asymmetric, it still generates forces as point functions.

- 3) In Fig. 5(b), when \mathbf{K}_1 is combined with ECT, the larger the selected c in terms of magnitude, the more asymmetric the Cartesian stiffness matrix will be, and the more the net work done after a closed path will deviate from the zero value.
- 4) Note that ECT does not always produce the exact Cartesian stiffness matrix. In Fig. 5(a), when \mathbf{K}_1 is combined with ECT, the resulting force is a point function. In contrast, when the asymmetric \mathbf{K}_2 is combined with ECT, the generated force is no longer a point function.
- 5) As stated in the previous conclusion, in general, a nonexact joint stiffness matrix will produce a nonexact Cartesian stiffness matrix (see Corollary 1). In Fig. 5(a), when \mathbf{K}_3 is combined with CCT, the resulting force is a point function. In contrast, when \mathbf{K}_4 is combined with CCT, the resulting force is no longer a point function.
- 6) In Fig. 5(b), since the selected joint stiffness matrices are all \mathbf{K}_1 , the work done in joint space for different stiffness mappings is all the same, which is shown as the blue dashed line. Only in the CCT case, the work done in joint space is equal to the work done in Cartesian space. The simulation result is consistent with Proposition 3.

B. Case 2: Stewart–Gough Platform

To illustrate the generality of the conclusions, we take the Stewart–Gough Platform as an example. As shown in Fig. 6, ΔOPQ is a fixed base, and Δrst is a floating platform moving in space. The six serial chains connecting the base to the moving platform are modeled as six translational springs. At every moment, the system can be considered to be in mechanical equilibrium under the action of external loads.

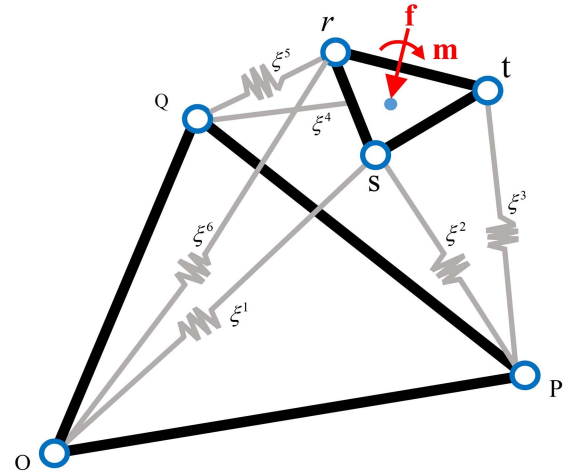


Fig. 6. Illustration of the Stewart-Gough Platform. The system elastic force is in equilibrium with the wrench acting on the moving platform Δrst .

In the simulation, the length of each spring is denoted as ξ^i ($i = 1, 2, \dots, 6$). The initial spring force of each spring is 10 N. Then the initial external forces and moments are calculated by the principle of virtual work. At the initial moment, the spatial coordinates of each point are as follows (Unit: m):

$$\begin{aligned} \mathbf{O} &= [0 \ 0 \ 0]^T, & \mathbf{P} &= [7 \ 0 \ 0]^T \\ \mathbf{Q} &= [3.5 \ 6 \ 0]^T, & \mathbf{r} &= [10 \ 4 \ 12]^T \\ \mathbf{s} &= [14 \ 8 \ 16]^T, & \mathbf{t} &= [14.5 \ 1.1 \ 16.5]^T. \end{aligned} \quad (69)$$

Two types of motions for the moving platform are considered: 1) purely translational motion and 2) spatial motion.

1) *Motion on $T(3)$* : When the motion is simply translational, the motion of the rigid body is then represented by a smooth curve on $T(3)$. In this case, after specifying the motion of any point on the moving platform, then the motion of the rigid body

is determined. In this simulation, the motion of the point \mathbf{s} (Unit: m) is specified as follows:

$$\begin{cases} \mathbf{s}(t) = \mathbf{s}_0 + 3 \begin{bmatrix} 1 & 0 & 0 \\ 0 & \frac{\sqrt{2}}{2} & -\frac{\sqrt{2}}{2} \\ 0 & \frac{\sqrt{2}}{2} & \frac{\sqrt{2}}{2} \end{bmatrix} \begin{bmatrix} \cos \alpha(t) - 1 \\ \sin \alpha(t) \\ 0 \end{bmatrix} \\ \alpha(t) \in [0, 2\pi]. \end{cases} \quad (70)$$

2) *Motion on SE(3)*: When the platform's motion contains translation and rotation, the motion of the rigid body is represented by the smooth curve on SE(3). In addition to specifying the spatial coordinates of one point on the rigid body, it is also necessary to give the orientation of the moving platform at each moment

$$\begin{cases} \mathbf{s}(t) = \mathbf{s}_0 + 3 \begin{bmatrix} 1 & 0 & 0 \\ 0 & \frac{\sqrt{2}}{2} & -\frac{\sqrt{2}}{2} \\ 0 & \frac{\sqrt{2}}{2} & \frac{\sqrt{2}}{2} \end{bmatrix} \begin{bmatrix} \cos \alpha(t) - 1 \\ \sin \alpha(t) \\ 0 \end{bmatrix} \\ \mathbf{R}(t) = \exp\left(\frac{\pi}{6} \sin \frac{\alpha(t)}{2} [\boldsymbol{\omega}(t)]\right) \mathbf{R}(0) \\ \boldsymbol{\omega}(t) = \left[\cos \frac{\pi}{4} \cos \frac{\alpha(t)}{2} \quad \sin \frac{\pi}{4} \cos \frac{\alpha(t)}{2} \quad \sin \frac{\alpha(t)}{2} \right]^T \\ \alpha(t) \in [0, 2\pi] \end{cases} \quad (71)$$

where $\mathbf{R}(t)$ is the rotation matrix of the moving platform with respect to the base coordinate system, $\exp(\cdot)$ is the matrix exponential function, and $[\boldsymbol{\omega}(t)]$ is the skew-symmetric matrix representation of the vector $\boldsymbol{\omega}(t)$.

Similar to the previous case, joint stiffness matrices \mathbf{K}_θ (Unit: N/m) with different properties and \mathbf{c} of different magnitudes are selected for simulation analysis

$$\mathbf{c}_1 = [0.5 \quad 0.5 \quad 0.5 \quad 0.5 \quad 0.5 \quad 0.5]^T \quad (72)$$

$$\mathbf{c}_2 = [1 \quad 1 \quad 1 \quad 1 \quad 1 \quad 1]^T \quad (73)$$

$$\mathbf{c}_3 = [1.5 \quad 1.5 \quad 1.5 \quad 1.5 \quad 1.5 \quad 1.5]^T \quad (74)$$

$$\mathbf{K}_1 = \text{diag}(1, 2, 3, 4, 5, 6) \quad (75)$$

$$\mathbf{K}_2 = \begin{bmatrix} 1 & 1 & 0 & 1 & 0 & 2 \\ 0 & 2 & 1 & 0 & 10 & 0 \\ 2 & 0 & 3 & 0 & 0 & 0 \\ 0 & 0 & 0 & 4 & 2 & 0 \\ 2 & 0 & 3 & 0 & 5 & 0 \\ 0 & 0 & 0 & 3 & 2 & 6 \end{bmatrix} \quad (76)$$

$$\mathbf{K}_3 = \text{diag}(5 \sin \xi^1, 10 \cos \xi^2, 3 \cos \xi^3, 2 \sin \xi^4, 2.5 \sin \xi^5, 3 \sin \xi^6) \quad (77)$$

$$\mathbf{K}_4 = \text{diag}(5 \sin \xi^3, 10 \cos \xi^1, 3 \cos \xi^2, 2 \sin \xi^6, 2.5 \sin \xi^4, 3 \sin \xi^5). \quad (78)$$

Similar to the case of the two-link manipulator, the Cartesian and joint stiffness matrices were used to calculate the forces and work of the system during motion. In this case, the calculation of force and work in joint space is the same as in (68c) and (68d). Since the 6-D motion consists of translation and rotation, we use the Jacobian matrix to convert the computation of force and

work in Cartesian space to integration over joint variables

$$\mathbf{f}(t) = \mathbf{f}(t-1) + \mathbf{K}_C \mathbf{J} d\xi \quad (79a)$$

$$W(t) = W(t-1) + \mathbf{f}(t)^T \mathbf{J} d\xi + \frac{1}{2} (\mathbf{J} d\xi)^T \mathbf{K}_C (\mathbf{J} d\xi). \quad (79b)$$

Fig. 7 shows the simulation of the Stewart–Gough Platform. $\alpha(t)$ changes from 0 to 2π (7200 simulation steps), and after a closed path, the moving platform returns to the initial state. For the case on $T(3)$, the force component f_x in the X direction is shown. The moment component m_z in the Z direction is selected for 6-D motion. Other components of the force or moment change in a similar pattern.

In this case, the size of the stiffness matrix is 6 by 6. In addition to the translational submatrix \mathbf{K}_{tt} describing the relationship between force and translational displacement, there are other submatrices relating to the rotation and moment

$$\mathbf{K}_{6 \times 6} = \begin{bmatrix} \mathbf{K}_{rr} & \mathbf{K}_{rt} \\ \mathbf{K}_{tr} & \mathbf{K}_{tt} \end{bmatrix}. \quad (80)$$

Here, \mathbf{K}_{tt} is arranged in the lower right corner, which is related to the way the Jacobian matrix is defined. It should be noted that comparing $T(3)$ and SE(3), the stiffness matrix changes not only in the dimensionality, but also the big difference is that the units of the matrix elements become inhomogeneous on SE(3). The difference between $T(3)$ and SE(3) makes the stiffness matrix on different manifolds exhibit different properties.

When the moving platform undergoes translational motion, the forces and the work done by the external forces are only related to \mathbf{K}_{tt} . At this point, the system is similar to the two-link system. When the motion of the moving platform is expanded to SE(3), the external load and the work done are related to each component of the 6×6 stiffness matrix.

Some observations are as follows:

- 1) In Fig. 7(a) and (b), the moving platform performs translational motion, and only the properties of \mathbf{K}_{tt} need to be considered. It is easy to check that the conclusions are the same as in Section VI-A.
- 2) When the joint stiffness matrix is exact, the resulting force is a point function regardless of whether the joint stiffness matrix is symmetric or not under CCT. The (CCT, \mathbf{K}_1), (CCT, \mathbf{K}_2), and (CCT, \mathbf{K}_3) cases in Fig. 7(c) confirm this statement. Here, (CCT, \mathbf{K}_θ) denotes the combination of CCT and \mathbf{K}_θ .
- 3) Comparing the (CCT, \mathbf{K}_1) and (CCT, \mathbf{K}_2) cases in Fig. 7(d), we can see that when the joint stiffness matrix is asymmetric, the work done by the system under CCT along the closed path is no longer zero.
- 4) Comparing the (CCT, \mathbf{K}_3) and (CCT, \mathbf{K}_4) cases in Fig. 7(d), we see that when the joint stiffness matrix is symmetric but nonexact, the work done by the system under CCT along the closed path is not zero.
- 5) As stated in Proposition 3, for an arbitrary joint stiffness matrix, CCT guarantees the equivalence of work done in joint space and Cartesian space. This is confirmed by the yellow and black dashed lines in Fig. 7(d).

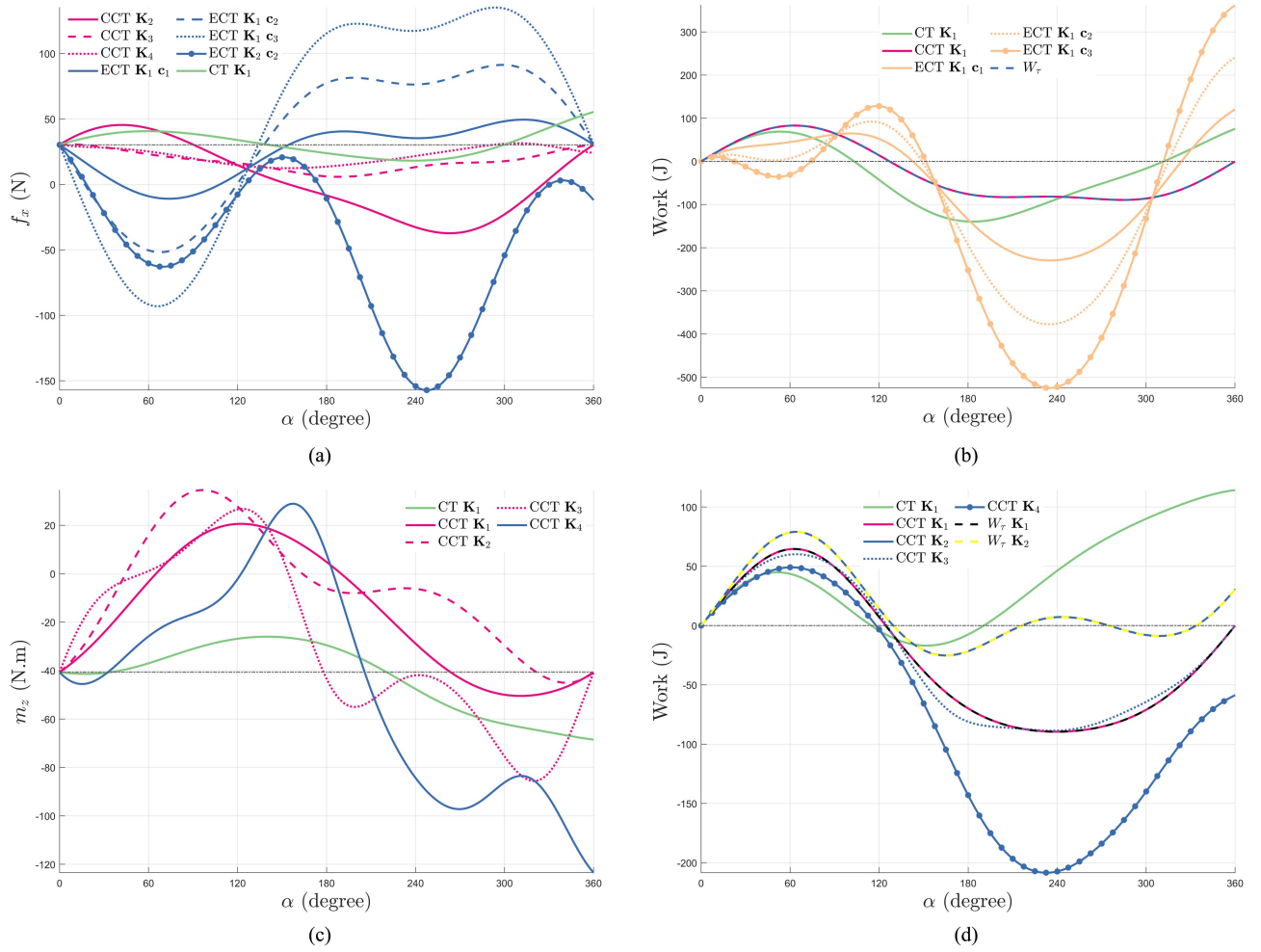


Fig. 7. Simulation of Stewart-Gough Platform for the joint-based control strategy: The parameter descriptions are given in Section VI-B. The figures show the external force and the work done on the closed path for (a) and (b) motion on $T(3)$ and (c) and (d) motion on $SE(3)$. (a) Force curves for motion on $T(3)$. (b) Work curves for motion on $T(3)$. The blue dashed line indicates the work done in joint space and the other lines indicate the work done in Cartesian space. (c) Force curves for motion on $SE(3)$. (d) Work curves for motion on $SE(3)$. The dashed line indicates the work done in joint space, and the other lines indicate the work done in Cartesian space.

6) In Fig. 8, the external loads applied during the motion of the rigid body are obtained using two different ways: 1) solving for the external loads using the numerical integration formula and 2) using the skew-symmetric components of the stiffness matrix to estimate the external loads. As can be seen from the figure, the force curves obtained from the two ways overlap exactly, verifying the correctness of (44) and (47).

With the above simulations, we verify the correctness and generality of the aforementioned corollaries and proposition.

VII. APPLICATION

A. Selection of the Connection

Tables II and III illustrate the corresponding stiffness mapping relationships for different connections and mechanical assumptions. In this section, we discuss the physical meaning and application of these formulas in practice.

For general industrial applications, the robot links are often considered rigid relative to the joints. Therefore, CT and CCT

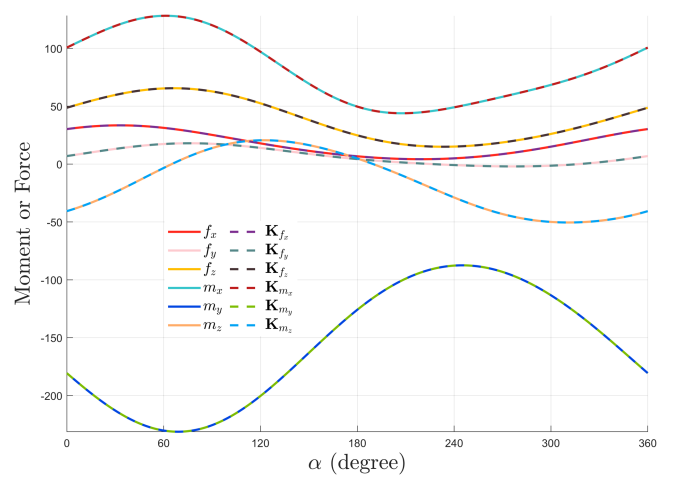


Fig. 8. Simulation of Stewart-Gough Platform for the joint-based control strategy: symmetric K_1 combined with CCT. The solid line indicates the value of the force or moment obtained by numerical integration, and the dashed line indicates the value of the force or moment obtained based on the stiffness matrix components according to (44) and (47).

models are the most widely used stiffness models. The physical implications of these different stiffness models can be summarized as follows:

- 1) CT: It is a simplified stiffness model suitable for practical applications. The effects of external forces as well as changes in Jacobian matrix are not considered in the model.
- 2) CCT: It is the precise stiffness model. The model degenerates to CT when the robotic system is not subjected to external forces or has a configuration-independent Jacobian (Cartesian gantry robot).
- 3) ECT: The model exists mathematically and is derived from the exactness of the stiffness matrix on $T(3)$. It does not correspond directly to the actual physical system.
- 4) Other stiffness models: These models consider mechanical conditions such as linkage flexibility and passive joints. As more factors are considered, the more complex the model becomes.

Depending on the characteristics of the different models, they can be applied to different specific tasks:

- 1) CT: Although CT is a simplified model, it is the most widely used in practice. The model is often used in evaluating the stiffness characteristics of the mechanism [54], compensating for static errors [55], optimizing the robot pose [56], and identifying robot stiffness parameters [57]. For general industrial applications, the model is concise and effective.
- 2) CCT: The model is suitable for applications where accuracy is required. In some literature, the model has been used to predict cutting forces as well as to avoid mode-coupled chattering in robotic machining [58], [59].
- 3) Other stiffness models: These models are used in applications such as stiffness parameter identification and error compensation for robots with special structures [60]. However, due to the complexity of these models, they are not widely used.

B. Application 1: Passivity-Based Control

We consider the robot rigid body dynamics under the generalized variables \mathbf{q} (robot joint angles or Cartesian positions)

$$\mathbf{M}(\mathbf{q})\ddot{\mathbf{q}} + \mathbf{C}(\mathbf{q}, \dot{\mathbf{q}})\dot{\mathbf{q}} + \mathbf{g}(\mathbf{q}) = \boldsymbol{\tau}_c + \boldsymbol{\tau}_e. \quad (81)$$

In interactive control scenarios, such as human–robot collaboration and robot polishing, designing a suitable control law to produce passive systems is an important issue. The goal is to preserve the passivity $(\boldsymbol{\tau}_e, \dot{\mathbf{q}})$ by designing a controller $\boldsymbol{\tau}_c$. The most common controller in practical applications can be expressed in the following form:

$$\boldsymbol{\tau}_c = \mathbf{g}(\mathbf{q}) - \mathbf{D}(\mathbf{q})\dot{\mathbf{q}} + \mathbf{f}(\mathbf{q}) \quad (82)$$

where $\mathbf{g}(\mathbf{q})$ is the gravity cancellation term, \mathbf{D} is a positive semidefinite matrix, and $\mathbf{f}(\mathbf{q})$ is the elastic force designed by the controller. Then, there is the following assertion about passivity [61], [62].

Lemma 2 (Kronander, Billard, [61]): Let $\mathbf{f}(\mathbf{q})$ be a conservative force, i.e., there exists a scalar function V_f such that $\mathbf{f}(\mathbf{q}) = -\nabla V_f(\mathbf{q})$. Then, the system (81) under control given by (82) is passive with respect to the input output pair $\boldsymbol{\tau}_e, \dot{\mathbf{q}}$ with the storage function $W(\mathbf{q}, \dot{\mathbf{q}}) = \frac{1}{2}\dot{\mathbf{q}}^T \mathbf{M}(\mathbf{q})\dot{\mathbf{q}} + V_f(\mathbf{q})$.

Using the results in Section IV, we can easily design a control strategy that allows reproducing a variable stiffness while preserving the passivity.

Proposition 6: The system (81) is passive under joint control law $\boldsymbol{\tau}_c(\boldsymbol{\xi})$ given by

$$\boldsymbol{\tau}_c(\boldsymbol{\xi}) = \mathbf{g}(\boldsymbol{\xi}) - \mathbf{D}(\boldsymbol{\xi})\dot{\boldsymbol{\xi}} + \int_{\boldsymbol{\xi}_0}^{\boldsymbol{\xi}} \mathbf{K}_{ctrl}(\boldsymbol{\xi})d\boldsymbol{\xi} \quad (83)$$

where \mathbf{K}_{ctrl} is symmetric and exact, i.e.,

$$[\mathbf{K}_{ctrl}]_{ij} = [\mathbf{K}_{ctrl}]_{ji}, \quad \frac{\partial[\mathbf{K}_{ctrl}]_{ki}}{\partial\xi^j} = \frac{\partial[\mathbf{K}_{ctrl}]_{kj}}{\partial\xi^i}. \quad (84)$$

Proof: When using the control law in (83), system (81) characterizes the joint stiffness with the value \mathbf{K}_{ctrl} . According to Proposition 4, the Cartesian stiffness matrix is conservative.

At this situation, the elastic force of the joint

$$\mathbf{f}(\boldsymbol{\xi}) = \int_{\boldsymbol{\xi}_0}^{\boldsymbol{\xi}} \mathbf{K}_{ctrl}(\boldsymbol{\xi})d\boldsymbol{\xi} \quad (85)$$

and the elastic force exhibited on the end-effector are all conservative. According to Lemma 2, the system is passive. \square

One of the simplest control laws can be set as

$$\begin{aligned} \mathbf{K}_{ctrl} \\ = \text{diag} (f_1 (\xi^1), f_2 (\xi^2), f_3 (\xi^3), f_4 (\xi^4), f_5 (\xi^5), f_6 (\xi^6)) \end{aligned} \quad (86)$$

where $f_i(\bullet)$ is a function of ξ^i .

Based on symmetry and exactness, we can design more complex joint control laws (e.g., joint stiffness matrix is non-diagonal) while preserving the passivity.

C. Application 2: Stiffness Identification

A cable-driven spherical joint module (CSJM) [63] is composed of a mobile platform, a base, a passive spherical joint, and cables. A six-axis force/torque sensor is fixed to the top of the mobile platform to measure external loads. At the same time, the pose of the moving platform is measured by a laser tracker.

The parallel mechanism is driven by six cables. Due to the constraint of the spherical joints, the moving platform exhibits three degrees of freedom of rotation. For such a redundant mechanism, the stiffness of the six cables cannot be identified by simply measuring the torque applied to the moving platform and the posture change it produces. So, we identify the stiffness matrix $\mathbf{K}_C \in \mathbb{R}^{3 \times 3}$ as a whole for a certain pose. The experimental data used in the article are from [63]. The posture \mathbf{R}_0 (moving platform with respect to the base) to be identified and the initial load \mathbf{m}_0 are shown in Table IV. Here, we use the precise stiffness model CCT for stiffness identification.

The results identified directly using least squares may be affected by environmental noise, resulting in the structure of the identified stiffness matrix often being inconsistent with the theoretical structure. So, we split the stiffness matrix into an skew-symmetric matrix \mathbf{K}_{skew} and a symmetric positive definite matrix \mathbf{K}_{pd} using the conclusions in Section IV-C

$$\mathbf{K}_C = \mathbf{K}_{pd} + \mathbf{K}_{skew} = \mathbf{K}_{pd} + \frac{1}{2}[\mathbf{m}] \quad (87)$$

TABLE IV
 STIFFNESS IDENTIFICATION RESULT

| Test posture \mathbf{R}_0 | Initial load \mathbf{m}_0 (Nm) | Identified stiffness matrix \mathbf{K}_C^* (Nm/rad) |
|---|---|--|
| $\begin{bmatrix} 0.9843 & -0.0807 & 0.1567 \\ 0.0764 & 0.9965 & 0.0332 \\ -0.1588 & -0.0207 & 0.9871 \end{bmatrix}$ | $\begin{bmatrix} 0.0705 \\ -2.4331 \\ 1.0767 \end{bmatrix}$ | $\begin{bmatrix} 18.4938 & 7.3535 & -1.5249 \\ 8.4302 & 27.5198 & -3.7162 \\ 0.9082 & -3.6457 & 13.6723 \end{bmatrix}$ |

where $\mathbf{K}_{\text{skew}} = \frac{1}{2}[\mathbf{m}]$ is obtained according to (45) in the case of SO(3).

In the experiment, we apply multiple sets of torques near the initial posture \mathbf{R}_0 , while recording the corresponding changes in the posture of the moving platform

$$\begin{aligned} [\Delta\mathbf{m}_1 \quad \cdots \quad \Delta\mathbf{m}_n] &= \mathbf{K}_C [\Delta\boldsymbol{\omega}_1 \quad \cdots \quad \Delta\boldsymbol{\omega}_n] \\ &= \left(\mathbf{K}_{pd} + \frac{1}{2}[\mathbf{m}_0] \right) [\Delta\boldsymbol{\omega}_1 \quad \cdots \quad \Delta\boldsymbol{\omega}_n] \end{aligned} \quad (88)$$

where $\Delta\mathbf{m}$ is the increment of torque, and $\Delta\boldsymbol{\omega}$ is the amount of change in posture under the axis-angle representation. The above physical quantities are expressed in body frame.

Equation (88) can be converted into the following form:

$$\mathbf{A} = \mathbf{K}_{pd}\mathbf{B} \quad (89)$$

where

$$\mathbf{A} = [\Delta\mathbf{m}_1 \quad \cdots \quad \Delta\mathbf{m}_n] - \frac{1}{2}[\mathbf{m}_0] [\Delta\boldsymbol{\omega}_1 \quad \cdots \quad \Delta\boldsymbol{\omega}_n] \quad (90)$$

$$\mathbf{B} = [\Delta\boldsymbol{\omega}_1 \quad \cdots \quad \Delta\boldsymbol{\omega}_n]. \quad (91)$$

Thus, the original identification problem can be transformed into an optimization problem defined on a positive definite manifold as follows:

$$\min_{\mathbf{K}_{pd} > 0} \text{tr} \left((\mathbf{A} - \mathbf{K}_{pd}\mathbf{B}) (\mathbf{A} - \mathbf{K}_{pd}\mathbf{B})^T \right). \quad (92)$$

In the experiment, 40 sets of data are used for identification, and (92) is solved by using the MATLAB toolbox *Manopt* [64]. After we get the optimal \mathbf{K}_{pd}^* for model (92), the identified stiffness matrix \mathbf{K}_C^* can be expressed as

$$\mathbf{K}_C^* = \mathbf{K}_{pd}^* + \frac{1}{2}[\mathbf{m}_0]. \quad (93)$$

Table IV shows the identified \mathbf{K}_C^* , which is consistent with the theoretical model.

By combining \mathbf{K}_C^* with the measured $\Delta\mathbf{m}$, we can predict the posture of the moving platform \mathbf{R}_{est} . Further comparing \mathbf{R}_{est} with \mathbf{R}_{real} measured by the laser tracker, we can assess the error E_θ in posture prediction

$$[\boldsymbol{\theta}_{\text{err}}] = \log \mathbf{R}_{\text{real}}^{-1} \mathbf{R}_{\text{est}}, E_\theta = \|\boldsymbol{\theta}_{\text{err}}\|. \quad (94)$$

We use 5 sets of data to test the pose estimation accuracy, as shown in Table V. It can be seen that the posture is estimated with high accuracy. Therefore, the \mathbf{K}_C^* identified by the above steps conforms to the physical model and can be used for practical applications.

 TABLE V
 STIFFNESS VERIFICATION RESULT

| Number | Load variation $\Delta\mathbf{m}$ (Nm) | Error E_θ (rad) |
|--------|--|------------------------|
| 1 | $\begin{bmatrix} 0.5295 & -0.4180 & -3.5344 \end{bmatrix}^T$ | 0.0499 |
| 2 | $\begin{bmatrix} 1.8026 & 1.1485 & -1.4490 \end{bmatrix}^T$ | 0.0609 |
| 3 | $\begin{bmatrix} 0.7633 & -0.0896 & -2.9031 \end{bmatrix}^T$ | 0.0678 |
| 4 | $\begin{bmatrix} 0.7895 & 2.4847 & 0.1006 \end{bmatrix}^T$ | 0.0683 |
| 5 | $\begin{bmatrix} 0.3956 & 0.3104 & -1.8300 \end{bmatrix}^T$ | 0.0187 |

VIII. CONCLUSION

In this article, the geometric framework for describing the stiffness of a conservative mechanical system is given. All current stiffness models can be unified in this geometric framework. After considering the geometric structure, the properties of the Cartesian stiffness matrix on SE(3) and the submanifold are easy to determine. We show that the nonzero Lie algebra structure constants cause the Cartesian stiffness matrix to be asymmetric under external forces. ECT, which generates an exact Cartesian stiffness matrix on $T(3)$, is obtained. CCT is shown to be the only stiffness mapping that generates a conservative Cartesian stiffness matrix on $T(3)$. Further, the conclusion of the conservative stiffness matrix is generalized to SE(3): a symmetric and exact joint stiffness matrix generates a conservative Cartesian stiffness matrix under CCT. Numerical simulations of different types of manipulators verify the correctness of the theory.

Through the above study of the conservativeness of the stiffness matrix, we design a variable stiffness impedance controller that guarantees passivity. Meanwhile, we propose a stiffness identification method for redundant cable-driven parallel robots using the structure of the skew-symmetric part of the stiffness matrix: experimental results show that the scheme has high accuracy while ensuring that the identification results conform to the physical model.

The theories and methods presented in this article can be applied in different fields. The following are the potential applications and directions for subsequent research. 1) Applying the passive control law proposed in this article combined with existing advanced control methods in physical human-robot interaction tasks. 2) Using the conclusions of this article on conservative stiffness to design suitable dynamic systems. 3) Further

exploring stiffness modeling in the geometric framework, e.g., principal axes decomposition of stiffness matrices.

APPENDIX

A. Proof of Corollary 2

Proof: We show that an exact and asymmetric joint stiffness matrix still generates an exact Cartesian stiffness matrix by CCT on $T(3)$.

In Section IV-A, the connection corresponding to CCT is obtained. Substituting (36) into (30), (30) is expressed as

$$\begin{aligned} \hat{\mathbf{L}}_k(K_{ij}^L) &= \left(\alpha_k^l \alpha_j^p \frac{\partial \alpha_i^m}{\partial \xi^p} + \alpha_k^p \alpha_j^l \frac{\partial \alpha_i^m}{\partial \xi^p} + \alpha_k^p \frac{\partial \alpha_j^l}{\partial \xi^p} \alpha_i^m \right) [\mathbf{K}_\theta]_{ml} \\ &\quad + \alpha_k^p \alpha_j^l \alpha_i^m \frac{\partial [\mathbf{K}_\theta]_{ml}}{\partial \xi^p} \\ &\quad + \left(\alpha_k^p \frac{\partial \alpha_j^l}{\partial \xi^p} \frac{\partial \alpha_i^n}{\partial \xi^l} + \alpha_k^p \alpha_j^l \frac{\partial^2 \alpha_i^n}{\partial \xi^p \partial \xi^l} \right) \tau_n \\ &= [\mathbf{C}_1]_{kji}^{lm} [\mathbf{K}_\theta]_{ml} + [\mathbf{C}_2]_{kji}^{plm} \frac{\partial [\mathbf{K}_\theta]_{ml}}{\partial \xi^p} + [\mathbf{C}_3]_{kji}^n \tau_n \end{aligned} \quad (95)$$

To prove that the Cartesian stiffness matrix is exact is to prove that (95) is symmetric with respect to the indexes j and k .

The symmetry of $[\mathbf{C}_2]_{kji}^{plm} \frac{\partial [\mathbf{K}_\theta]_{ml}}{\partial \xi^p}$ is ensured by the exactness of the joint stiffness matrix.

Parameterizing the coordinates on $T(3)$ as x^i ($i = 4, 5, 6$), then

$$\alpha_k^p = \frac{\partial \xi^p}{\partial x^k}. \quad (96)$$

Thus, $[\mathbf{C}_1]_{kji}^{lm}$ and $[\mathbf{C}_3]_{kji}^n$ can be expressed as

$$[\mathbf{C}_1]_{kji}^{lm} = \left(\alpha_k^l \alpha_j^p \frac{\partial \alpha_i^m}{\partial \xi^p} + \alpha_k^p \alpha_j^l \frac{\partial \alpha_i^m}{\partial \xi^p} \right) + \frac{\partial^2 \xi^l}{\partial x^k \partial x^j} \alpha_i^m \quad (97)$$

$$[\mathbf{C}_3]_{kji}^n = \frac{\partial^2 \xi^l}{\partial x^k \partial x^j} \frac{\partial \alpha_i^n}{\partial \xi^l} + \alpha_k^p \alpha_j^l \frac{\partial^2 \alpha_i^n}{\partial \xi^p \partial \xi^l}. \quad (98)$$

Since the Lie bracket between the vector fields vanishes on $T(3)$, i.e., $\left[\frac{\partial}{\partial \xi^i}, \frac{\partial}{\partial \xi^j} \right] = 0$, $\left[\frac{\partial}{\partial x^i}, \frac{\partial}{\partial x^j} \right] = 0$, the partial derivatives can be exchanged: $\frac{\partial^2(\cdot)}{\partial x^i \partial x^j} = \frac{\partial^2(\cdot)}{\partial x^j \partial x^i}$, $\frac{\partial^2(\cdot)}{\partial \xi^i \partial \xi^j} = \frac{\partial^2(\cdot)}{\partial \xi^j \partial \xi^i}$. It is easy to check that (97) and (98) is symmetric with respect to the indexes j and k .

By the above analysis, all parts of (95) are symmetric about the indexes j and k . Therefore, (95) is symmetric. \square

B. Proof of Proposition 3

Proof: The following content proves that the work done in the joint space is equal to the work done by the external wrench under CCT.

The CCT formula can be rewritten as

$$\mathbf{J}^T \mathbf{K}_C \mathbf{J} d\xi = \mathbf{K}_\theta d\xi - \mathbf{K}_g d\xi. \quad (99)$$

Notice that $\mathbf{K}_g d\xi$ can be rewritten as

$$\begin{aligned} \mathbf{K}_g d\xi &= \left[\left(\frac{\partial \mathbf{J}^T}{\partial \xi^1} \mathcal{F} \right) \left(\frac{\partial \mathbf{J}^T}{\partial \xi^2} \mathcal{F} \right) \cdots \left(\frac{\partial \mathbf{J}^T}{\partial \xi^n} \mathcal{F} \right) \right] d\xi \\ &= \left(\frac{\partial \mathbf{J}^T}{\partial \xi^i} \mathcal{F} \right) d\xi^i = \left(\frac{\partial \mathbf{J}^T}{\partial \xi^i} d\xi^i \right) \mathcal{F} = d\mathbf{J}^T \mathcal{F}. \end{aligned} \quad (100)$$

Then (99) can be expressed as

$$\begin{aligned} \mathbf{0} &= \mathbf{J}^T \mathbf{K}_C \mathbf{J} d\xi - \mathbf{K}_\theta d\xi + \mathbf{K}_g d\xi \\ &= \mathbf{J}^T d\mathcal{F} - d\tau + d\mathbf{J}^T \mathcal{F} \\ &= d(\mathbf{J}^T \mathcal{F} - \tau). \end{aligned} \quad (101)$$

In real physical systems as well as in simulation calculations, the initial conditions satisfy the principle of virtual work $\mathbf{J}_0^T \mathcal{F}_0 = \tau_0$, which means $\mathbf{J}^T \mathcal{F} \equiv \tau$. The principle of virtual work means that the work done by the joint torque is equal to the work done by the external force. \square

C. Proof of Proposition 4

Proof: Next, we prove that the exact and symmetric \mathbf{K}_θ corresponds to the conservative \mathbf{K}_C under CCT on $SE(3)$.

1) The differential element of the wrench $d\mathcal{F}$ under CCT can be represented as

$$d\mathcal{F} = \mathbf{K}_C \mathbf{J} d\xi = \mathbf{J}^{-T} (\mathbf{K}_\theta - \mathbf{K}_g) d\xi. \quad (102)$$

The component representation of (102) is

$$\begin{aligned} d\mathcal{F}_q &= \alpha_q^k \left([\mathbf{K}_\theta]_{kj} - \frac{\partial \gamma_k^p}{\partial \xi^j} \alpha_p^m \tau_m \right) d\xi^j \\ &= \omega = \omega_j d\xi^j \end{aligned} \quad (103)$$

where ω can be considered as the 1-form. Then

$$\begin{aligned} \frac{\partial \omega_j}{\partial \xi^i} &= \frac{\partial \alpha_q^m}{\partial \xi^i} [\mathbf{K}_\theta]_{mj} - \alpha_q^k \frac{\partial \gamma_k^p}{\partial \xi^j} \alpha_p^m [\mathbf{K}_\theta]_{mi} \\ &\quad + \alpha_q^k \frac{\partial [\mathbf{K}_\theta]_{kj}}{\partial \xi^i} - \frac{\partial \left(\alpha_q^k \alpha_p^m \frac{\partial \gamma_k^p}{\partial \xi^j} \right)}{\partial \xi^i} \tau_m. \end{aligned} \quad (104)$$

Notice that

$$\frac{\partial \gamma_k^p}{\partial \xi^j} \alpha_p^m = - \frac{\partial \alpha_p^m}{\partial \xi^j} \gamma_k^p \quad (105)$$

$$\alpha_q^k \frac{\partial \gamma_k^p}{\partial \xi^j} \alpha_p^m = - \frac{\partial \alpha_p^m}{\partial \xi^j} \gamma_k^p \alpha_q^k = - \frac{\partial \alpha_q^m}{\partial \xi^j} \quad (106)$$

then (104) can be simplified as

$$\begin{aligned} \frac{\partial \omega_j}{\partial \xi^i} &= \left(\frac{\partial \alpha_q^m}{\partial \xi^i} [\mathbf{K}_\theta]_{mj} + \frac{\partial \alpha_q^m}{\partial \xi^j} [\mathbf{K}_\theta]_{mi} \right) \\ &\quad + \frac{\partial \alpha_q^m}{\partial \xi^i \partial \xi^j} \tau_m + \alpha_q^k \frac{\partial [\mathbf{K}_\theta]_{kj}}{\partial \xi^i}. \end{aligned} \quad (107)$$

The terms $\left(\frac{\partial \alpha_q^m}{\partial \xi^i} [\mathbf{K}_\theta]_{mj} + \frac{\partial \alpha_q^m}{\partial \xi^j} [\mathbf{K}_\theta]_{mi} \right)$ and $\frac{\partial \alpha_q^m}{\partial \xi^i \partial \xi^j} \tau_m$ are symmetric with respect to indicators i and j .

When \mathbf{K}_θ is exact

$$\frac{\partial \omega_i}{\partial \xi^j} = \frac{\partial \omega_j}{\partial \xi^i}. \quad (108)$$

This means ω is a closed form

$$d\omega = \frac{\partial\omega_j}{\partial\xi^i} d\xi^i \wedge d\xi^j = 0. \quad (109)$$

According to the Poincaré lemma, ω is an exact form, then

$$\oint_{\partial\Sigma} \omega = 0 = \oint_{\partial\Sigma} d\mathcal{F}_q = \mathcal{F}_q \quad (110)$$

$$\oint_{\partial\Sigma} d\mathcal{F} = \mathcal{F} = \mathbf{0}. \quad (111)$$

- 2) According to Proposition 3, the work done in the joint space W_τ is equal to the work done by the external wrench $W_{\mathcal{F}}$ under CCT. So, we study the work done by the joint torque

$$dW = \tau_i d\xi^i = \sigma. \quad (112)$$

When \mathbf{K}_θ is symmetric, σ is a closed form

$$d\sigma = \frac{\partial\tau_i}{\partial\xi^j} d\xi^j \wedge d\xi^i = [\mathbf{K}_\theta]_{ij} d\xi^j \wedge d\xi^i = 0. \quad (113)$$

Similarly, we derive

$$\oint_{\partial\Sigma} \sigma = 0 = \oint_{\partial\Sigma} dW = W. \quad (114)$$

- 3) In summary, we have the following conclusions:

$$\begin{cases} \frac{\partial[\mathbf{K}_\theta]_{ki}}{\partial\xi^j} = \frac{\partial[\mathbf{K}_\theta]_{kj}}{\partial\xi^i}, \\ [\mathbf{K}_\theta]_{ij} = [\mathbf{K}_\theta]_{ji}. \end{cases} \Rightarrow \begin{cases} \mathcal{F} = \oint_{\partial\Sigma} d\mathcal{F} = \mathbf{0}, \\ W = \oint_{\partial\Sigma} dW = 0. \end{cases} \quad (115)$$

□

D. Proof of Proposition 5

Proof: The following content proves that the exact and symmetric joint stiffness matrix \mathbf{K}_θ generates the Cartesian stiffness matrix \mathbf{K}_C such that the wrench \mathcal{F} is a point function under ECT on SE(3).

The differential element of the wrench $d\mathcal{F}$ under ECT can be represented as

$$d\mathcal{F} = \mathbf{K}_C \mathbf{J} d\xi = \mathbf{J}^{-T} (\mathbf{K}_\theta - \mathbf{K}_g) d\xi - \mathbf{c}\tau^T d\xi. \quad (116)$$

The component representation of (116) is

$$\begin{aligned} d\mathcal{F}_q &= \alpha_q^k \left([\mathbf{K}_\theta]_{kj} - \frac{\partial\gamma_k^p}{\partial\xi^j} \alpha_p^m \tau_m \right) d\xi^j - c_q \tau_j d\xi^j \\ &= \omega = \omega_j d\xi^j. \end{aligned} \quad (117)$$

Similar to (107), we get

$$\begin{aligned} \frac{\partial\omega_j}{\partial\xi^i} &= \left(\frac{\partial\alpha_q^m}{\partial\xi^i} [\mathbf{K}_\theta]_{mj} + \frac{\partial\alpha_q^m}{\partial\xi^j} [\mathbf{K}_\theta]_{mi} \right) \\ &+ \frac{\partial\alpha_q^m}{\partial\xi^i \partial\xi^j} \tau_m + \alpha_q^k \frac{\partial[\mathbf{K}_\theta]_{kj}}{\partial\xi^i} - c_q [\mathbf{K}_\theta]_{ji}. \end{aligned} \quad (118)$$

When \mathbf{K}_θ is exact and symmetric

$$\frac{\partial\omega_i}{\partial\xi^j} = \frac{\partial\omega_j}{\partial\xi^i}. \quad (119)$$

According to (109)–(111), we get

$$\oint_{\partial\Sigma} d\mathcal{F} = \mathcal{F} = \mathbf{0}. \quad (120)$$

□

E. Stiffness Modeling for Passive Joints

Here, we follow the assumptions in [25]: consider the elasticity of the active joints ξ and passive joints λ . The Jacobian matrix between the active and passive joints is defined as

$$\frac{\partial\lambda}{\partial\xi} = \mathbf{G}, [\mathbf{G}]_{ij} = \beta_j^i \quad (121)$$

and the elastic potential energy of the system can be expressed as

$$\Phi = \int_{\xi_0}^{\xi} \tau_\xi^T d\xi + \int_{\lambda_0}^{\lambda} \tau_\lambda^T \mathbf{G} d\xi + \Phi_0. \quad (122)$$

Then

$$E_i(\Phi) = \frac{\partial\Phi}{\partial\xi^i} = \tau_{\xi_i} + \beta_i^k \tau_{\lambda_k} \quad (123)$$

$$E_j E_i(\Phi) = \frac{\partial\tau_{\xi_i}}{\partial\xi^j} + \frac{\partial\beta_i^k}{\partial\xi^j} \tau_{\lambda_k} + \beta_i^k \frac{\partial\tau_{\lambda_k}}{\partial\xi^j}. \quad (124)$$

Here, we select the connection ${}^L\Gamma_{ij}^m \equiv 0$. Combining (123), (124), and (34), we get

$$K_{ij}^L = \alpha_i^k \left[\frac{\partial\tau_{\xi_k}}{\partial\xi^l} + \frac{\partial\beta_k^p}{\partial\xi^l} \tau_{\lambda_p} + \beta_k^p \frac{\partial\tau_{\lambda_p}}{\partial\xi^l} - \frac{\partial\gamma_k^p}{\partial\xi^l} \mathcal{F}_p \right] \alpha_j^l. \quad (125)$$

Notice that

$$\frac{\tau_{\xi_k}}{\partial\xi^l} = [\mathbf{K}_\theta]_{kl}, \frac{\partial\tau_{\lambda_p}}{\partial\xi^l} = \frac{\partial\tau_{\lambda_p}}{\partial\lambda^q} \frac{\partial\lambda^q}{\partial\xi^l} = [\mathbf{K}_\lambda]_{pq} \beta_l^q. \quad (126)$$

Then

$$K_{ij}^L = \alpha_i^k \left[[\mathbf{K}_\theta]_{kl} + \frac{\partial\beta_k^p}{\partial\xi^l} \tau_{\lambda_p} + \beta_k^p [\mathbf{K}_\lambda]_{pq} \beta_l^q - \frac{\partial\gamma_k^p}{\partial\xi^l} \mathcal{F}_p \right] \alpha_j^l. \quad (127)$$

Then (127) can be expressed in matrix form (see [25]):

$$\begin{aligned} \mathbf{K}_C &= \mathbf{J}^{-T} \left(\mathbf{K}_\theta + \frac{\partial\mathbf{G}^T}{\partial\xi} \tau_\lambda + \mathbf{G}^T \mathbf{K}_\lambda \mathbf{G} - \frac{\partial\mathbf{J}^T}{\partial\xi} \mathcal{F} \right) \mathbf{J}^{-1} \\ &= \mathbf{J}^{-T} (\mathbf{K}_\theta + \mathbf{K}_I - \mathbf{K}_g) \mathbf{J}^{-1}. \end{aligned} \quad (128)$$

F. Stiffness Modeling for Flexible Links

Here, we follow the assumptions and notations in [12], [13], and [16]: the actuator and linkages are seen as the flexible active joints θ , and the kinematic pairs are seen as the passive joints \mathbf{q} without flexibility. The location of the end-effector \mathbf{T} and the variation dt it produces can be expressed as

$$\mathbf{T} = \mathbf{T}(\theta^1, \theta^2, \dots, \theta^n; q^1, q^2, \dots, q^s) \quad (129)$$

$$d\mathbf{T} = \mathbf{J}_\theta d\theta + \mathbf{J}_q dq. \quad (130)$$

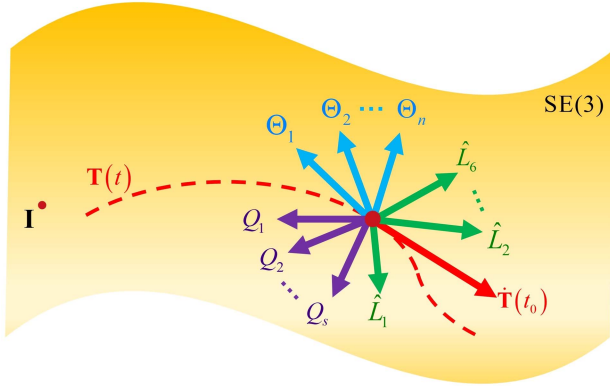


Fig. 9. Schematic of the vector fields on $SE(3)$. $\mathbf{T}(t)$ is a smooth curve on $SE(3)$, which represents continuous rigid body motion. $\dot{\mathbf{T}}(t_0)$ is the velocity of motion at t_0 , which can be expressed as a linear combination of vectors in the tangent space at $\mathbf{T}(t_0)$.

Then we have

$$\begin{aligned} d\mathbf{T} &= \frac{\partial \mathbf{T}}{\partial \theta^i} d\theta^i + \frac{\partial \mathbf{T}}{\partial q^j} dq^j = d\theta^i \Theta_i + dq^j Q_j \\ &= dt^k \hat{\mathbf{L}}_k = \left(\gamma_{\theta_i}^k d\theta^i + \gamma_{q_j}^k dq^j \right) \hat{\mathbf{L}}_k \end{aligned} \quad (131)$$

where Θ_i and Q_j can be seen as the vector fields on $SE(3)$, as shown in Fig. 9. From (131), we know that for any $d\theta^i$ and dq^j the following equation holds:

$$d\theta^i \left(\Theta_i - \gamma_{\theta_i}^k \hat{\mathbf{L}}_k \right) + dq^j \left(Q_j - \gamma_{q_j}^k \hat{\mathbf{L}}_k \right) = \mathbf{0} \quad (132)$$

thus, $\Theta_i = \gamma_{\theta_i}^k \hat{\mathbf{L}}_k$, $Q_j = \gamma_{q_j}^k \hat{\mathbf{L}}_k$.

1) *Case 1*: When considering the elasticity of the active joint, the potential energy of the system is expressed as

$$\Phi = \int_{\theta_0}^{\theta} \boldsymbol{\tau}^T d\boldsymbol{\theta} + \Phi_0. \quad (133)$$

Then, we have

$$\langle d\Phi, \Theta_i \rangle = \tau_i = \langle d\Phi, \gamma_{\theta_i}^k \hat{\mathbf{L}}_k \rangle = \gamma_{\theta_i}^k \mathcal{F}_k \quad (134)$$

$$\langle d\Phi, Q_j \rangle = 0 = \langle d\Phi, \gamma_{q_j}^k \hat{\mathbf{L}}_k \rangle = \gamma_{q_j}^k \mathcal{F}_k. \quad (135)$$

The above equations can be converted into the form of matrix

$$\begin{cases} \boldsymbol{\tau} = \mathbf{J}_{\theta}^T \mathcal{F} \\ \mathbf{0} = \mathbf{J}_{q}^T \mathcal{F}. \end{cases} \quad (136)$$

Differentiate both sides of (136)

$$\begin{cases} d\boldsymbol{\tau} = d\mathbf{J}_{\theta}^T \mathcal{F} + \mathbf{J}_{\theta}^T d\mathcal{F} \\ \mathbf{0} = d\mathbf{J}_{q}^T \mathcal{F} + \mathbf{J}_{q}^T d\mathcal{F}. \end{cases} \quad (137)$$

Notice that

$$\begin{aligned} d\mathbf{J}_{\theta}^T \mathcal{F} &= \left(\frac{\partial \mathbf{J}_{\theta}^T}{\partial \theta^i} \mathcal{F} \right) d\theta^i + \left(\frac{\partial \mathbf{J}_{\theta}^T}{\partial q^j} \mathcal{F} \right) dq^j \\ &= \mathbf{H}_{\theta\theta}^{\mathcal{F}} d\boldsymbol{\theta} + \mathbf{H}_{\theta q}^{\mathcal{F}} dq^j \end{aligned} \quad (138)$$

$$d\mathbf{J}_{q}^T \mathcal{F} = \left(\frac{\partial \mathbf{J}_{q}^T}{\partial \theta^i} \mathcal{F} \right) d\theta^i + \left(\frac{\partial \mathbf{J}_{q}^T}{\partial q^j} \mathcal{F} \right) dq^j$$

$$= \mathbf{H}_{q\theta}^{\mathcal{F}} d\boldsymbol{\theta} + \mathbf{H}_{qq}^{\mathcal{F}} dq^j. \quad (139)$$

Then, (137) can be expressed as

$$\begin{cases} d\boldsymbol{\tau} = \mathbf{H}_{\theta\theta}^{\mathcal{F}} d\boldsymbol{\theta} + \mathbf{H}_{\theta q}^{\mathcal{F}} dq^j + \mathbf{J}_{\theta}^T d\mathcal{F} \\ \mathbf{0} = \mathbf{H}_{q\theta}^{\mathcal{F}} d\boldsymbol{\theta} + \mathbf{H}_{qq}^{\mathcal{F}} dq^j + \mathbf{J}_{q}^T d\mathcal{F}. \end{cases} \quad (140)$$

Combining (140) with (130), we obtain

$$\begin{bmatrix} \mathbf{0} & \mathbf{J}_{q} & \mathbf{J}_{\theta} \\ \mathbf{J}_{q}^T & \mathbf{H}_{qq}^{\mathcal{F}} & \mathbf{H}_{q\theta}^{\mathcal{F}} \\ \mathbf{J}_{\theta}^T & \mathbf{H}_{\theta q}^{\mathcal{F}} & \mathbf{H}_{\theta\theta}^{\mathcal{F}} - \mathbf{K}_{\theta} \end{bmatrix} \begin{bmatrix} d\mathcal{F} \\ dq^j \\ d\boldsymbol{\theta} \end{bmatrix} = \begin{bmatrix} dt \\ \mathbf{0} \\ \mathbf{0} \end{bmatrix}. \quad (141)$$

Finally, we get the expression of \mathbf{K}_C (see [13]):

$$\begin{bmatrix} \mathbf{K}_C & * & * \\ * & * & * \\ * & * & * \end{bmatrix} = \begin{bmatrix} \mathbf{0} & \mathbf{J}_{q} & \mathbf{J}_{\theta} \\ \mathbf{J}_{q}^T & \mathbf{H}_{qq}^{\mathcal{F}} & \mathbf{H}_{q\theta}^{\mathcal{F}} \\ \mathbf{J}_{\theta}^T & \mathbf{H}_{\theta q}^{\mathcal{F}} & \mathbf{H}_{\theta\theta}^{\mathcal{F}} - \mathbf{K}_{\theta} \end{bmatrix}^{-1}. \quad (142)$$

It can be checked that the process of (136)–(137) implies the connection ${}^L\Gamma_{ij}^m \equiv 0$.

2) *Case 2*: When considering the elasticity of the active joint, the potential energy is the same as (133). Combining (130) with (136), we get

$$dt = \mathbf{J}_{\theta} \mathbf{K}_{\theta}^{-1} \mathbf{J}_{\theta}^T \mathcal{F} + \mathbf{J}_{q} dq^j. \quad (143)$$

Combining (136) with (143), we get

$$\begin{bmatrix} \mathbf{J}_{\theta} \mathbf{K}_{\theta}^{-1} \mathbf{J}_{\theta}^T & \mathbf{J}_{q} \\ \mathbf{J}_{q}^T & \mathbf{0} \end{bmatrix} \begin{bmatrix} \mathcal{F} \\ dq^j \end{bmatrix} = \begin{bmatrix} dt \\ \mathbf{0} \end{bmatrix}. \quad (144)$$

So \mathbf{K}_C (see [12]) is as follows:

$$\begin{bmatrix} \mathbf{K}_C & * \\ * & * \end{bmatrix} = \begin{bmatrix} \mathbf{J}_{\theta} \mathbf{K}_{\theta}^{-1} \mathbf{J}_{\theta}^T & \mathbf{J}_{q} \\ \mathbf{J}_{q}^T & \mathbf{0} \end{bmatrix}^{-1}. \quad (145)$$

It can be checked that (143) implies the connection ${}^E\Gamma_{ij}^m \equiv 0$.

3) *Case 3*: Now comes the more complex case: consider the effect of gravity on stiffness. Suppose there are e nodes in the system that need to consider gravity $\mathbf{G}_l (l = 1, 2, \dots, e)$. Then, the potential energy function of the system is described as

$$\Phi = \int_{\theta_0}^{\theta} \boldsymbol{\tau}^T d\boldsymbol{\theta} - \int \mathbf{G}_l^T dt^l + \Phi_0. \quad (146)$$

The rest of the derivation steps are the same as in Case 1. We obtain an equation similar to (142) (see [16]):

$$\begin{bmatrix} \mathbf{K}_C & * & * \\ * & * & * \\ * & * & * \end{bmatrix} = \begin{bmatrix} \mathbf{0} & \mathbf{J}_{q} & \mathbf{J}_{\theta} \\ \mathbf{J}_{q}^T & \mathbf{H}_{qq}^{\mathcal{F}} & \mathbf{H}_{q\theta}^{\mathcal{F}} \\ \mathbf{J}_{\theta}^T & \mathbf{H}_{\theta q}^{\mathcal{F}} & \mathbf{H}_{\theta\theta}^{\mathcal{F}} - \mathbf{K}_{\theta} \end{bmatrix}^{-1}. \quad (147)$$

ACKNOWLEDGMENT

Tengyu Hou would like to thank Prof. Tudor Ratiu for his class on the Lie group theory and would also like to thank Dr. Kaisheng Yang for providing the experimental data.

REFERENCES

- [1] F. M. Dimentberg, "The screw calculus and its applications in mechanics," Foreign Technology Division, Wright-Patterson Air Force Base, Dayton, OH, USA, Document No. FTD-HT-23-1632-67, 1965.

- [2] R. S. Ball, *A Treatise on the Theory of Screws*. Cambridge, U.K.: Cambridge Univ. Press, 1900.
- [3] J. Lončarić, “Geometrical analysis of compliant mechanisms in robotics,” Ph.D. dissertation, Sch. Eng. Appl. Sci., Harvard Univ., Cambridge, MA, USA, 1985.
- [4] B. S. El-Khasawneh and P. M. Ferreira, “Computation of stiffness and stiffness bounds for parallel link manipulators,” *Int. J. Mach. Tools Manufacture*, vol. 39, no. 2, pp. 321–342, 1999.
- [5] J. E. Akin, *Finite Element Analysis With Error Estimators: An Introduction to the FEM and Adaptive Error Analysis for Engineering Students*. Burlington, NJ, USA: Butterworth-Heinemann, 2005.
- [6] A. Klimchik, A. Pashkevich, and D. Chablat, “CAD-based approach for identification of elasto-static parameters of robotic manipulators,” *Finite Elements Anal. Des.*, vol. 75, pp. 19–30, 2013.
- [7] T. Huang, X. Zhao, and D. J. Whitehouse, “Stiffness estimation of a tripod-based parallel kinematic machine,” *IEEE Trans. Robot. Autom.*, vol. 18, no. 1, pp. 50–58, Feb. 2002.
- [8] H. C. Martin, *Introduction to Matrix Methods of Structural Analysis*. New York, NY, USA: McGraw-Hill, 1966.
- [9] D. Deblaise, X. Hernot, and P. Maurine, “A systematic analytical method for PKM stiffness matrix calculation,” in *Proc. IEEE Int. Conf. Robot. Automat.*, 2006, pp. 4213–4219.
- [10] G. Yu, L. Wang, J. Wu, D. Wang, and C. Hu, “Stiffness modeling approach for a 3-DOF parallel manipulator with consideration of non-linear joint stiffness,” *Mechanism Mach. Theory*, vol. 123, pp. 137–152, 2018.
- [11] A. Klimchik, A. Pashkevich, and D. Chablat, “Fundamentals of manipulator stiffness modeling using matrix structural analysis,” *Mechanism Mach. Theory*, vol. 133, pp. 365–394, 2019.
- [12] A. Pashkevich, D. Chablat, and P. Wenger, “Stiffness analysis of overconstrained parallel manipulators,” *Mechanism Mach. Theory*, vol. 44, no. 5, pp. 966–982, 2009.
- [13] A. Pashkevich, A. Klimchik, and D. Chablat, “Enhanced stiffness modeling of manipulators with passive joints,” *Mechanism Mach. Theory*, vol. 46, no. 5, pp. 662–679, 2011.
- [14] C. Quenouelle and C. M. Gosselin, “A general formulation for the stiffness matrix of parallel mechanisms,” 2012, *arXiv:1212.0950*.
- [15] A. Klimchik, A. Pashkevich, S. Caro, and D. Chablat, “Stiffness matrix of manipulators with passive joints: Computational aspects,” *IEEE Trans. Robot.*, vol. 28, no. 4, pp. 955–958, Aug. 2012.
- [16] A. Klimchik, D. Chablat, and A. Pashkevich, “Stiffness modeling for perfect and non-perfect parallel manipulators under internal and external loadings,” *Mechanism Mach. Theory*, vol. 79, pp. 1–28, 2014.
- [17] J. K. Salisbury, “Active stiffness control of a manipulator in Cartesian coordinates,” in *Proc. IEEE 19th Conf. Decis. Control Including Symp. Adaptive Processes*, 1980, pp. 95–100.
- [18] C. Gosselin, “Stiffness mapping for parallel manipulators,” *IEEE Trans. Robot. Autom.*, vol. 6, no. 3, pp. 377–382, Jun. 1990.
- [19] D. Zhang, F. Xi, C. M. Mechevske, and S. Y. Lang, “Analysis of parallel kinematic machine with kinetostatic modelling method,” *Robot. Comput.-Integr. Manuf.*, vol. 20, no. 2, pp. 151–165, 2004.
- [20] F. Xi, D. Zhang, C. M. Mechevske, and S. Y. Lang, “Global kinetostatic modelling of tripod-based parallel kinematic machine,” *Mechanism Mach. Theory*, vol. 39, no. 4, pp. 357–377, 2004.
- [21] S.-F. Chen and I. Kao, “Conservative congruence transformation for joint and Cartesian stiffness matrices of robotic hands and fingers,” *Int. J. Robot. Res.*, vol. 19, no. 9, pp. 835–847, 2000.
- [22] C. Huang, W.-H. Hung, and I. Kao, “New conservative stiffness mapping for the Stewart-Gough platform,” in *Proc. IEEE Int. Conf. Robot. Automat.*, 2002, pp. 823–828.
- [23] G. Alici and B. Shirinzadeh, “Enhanced stiffness modeling, identification and characterization for robot manipulators,” *IEEE Trans. Robot.*, vol. 21, no. 4, pp. 554–564, Aug. 2005.
- [24] C. Quenouelle and C. M. Gosselin, “Instantaneous kinemato-static model of planar compliant parallel mechanisms,” in *Proc. Int. Des. Eng. Tech. Conf. Comput. Inf. Eng. Conf.*, 2008, pp. 163–173.
- [25] C. Quenouelle and C. M. Gosselin, “Stiffness matrix of compliant parallel mechanisms,” in *Proc. Int. Des. Eng. Tech. Conf. Comput. Inf. Eng. Conf.*, 2008, pp. 151–161.
- [26] B.-J. Yi and R. A. Freeman, “Synthesis of actively adjustable springs by antagonistic redundant actuation,” *ASME J. Dyn. Syst. Meas. Control B*, vol. 114, no. 3, pp. 454–461, 1992.
- [27] B.-J. Yi and R. A. Freeman, “Geometric analysis of antagonistic stiffness in redundantly actuated parallel mechanisms,” *J. Robot. Syst.*, vol. 10, no. 5, pp. 581–603, 1993.
- [28] M. Wang, H. Liu, T. Huang, and D. G. Chetwynd, “Compliance analysis of a 3-SPR parallel mechanism with consideration of gravity,” *Mechanism Mach. Theory*, vol. 84, pp. 99–112, 2015.
- [29] Y. Li, H. Liu, X. Zhao, T. Huang, and D. G. Chetwynd, “Design of a 3-DOF PKM module for large structural component machining,” *Mechanism Mach. Theory*, vol. 45, no. 6, pp. 941–954, 2010.
- [30] B. Lian, T. Sun, Y. Song, Y. Jin, and M. Price, “Stiffness analysis and experiment of a novel 5-DOF parallel kinematic machine considering gravitational effects,” *Int. J. Mach. Tools Manufacture*, vol. 95, pp. 82–96, 2015.
- [31] M. Wang, H. Liu, and T. Huang, “An approach for the lightweight design of a 3-SPR parallel mechanism,” *J. Mechanisms Robot.*, vol. 9, no. 5, 2017, Art. no. 051016.
- [32] W.-A. Cao and H. Ding, “A method for stiffness modeling of 3R2T overconstrained parallel robotic mechanisms based on screw theory and strain energy,” *Precis. Eng.*, vol. 51, pp. 10–29, 2018.
- [33] W.-A. Cao, D. Yang, and H. Ding, “A method for stiffness analysis of overconstrained parallel robotic mechanisms with Scara motion,” *Robot. Comput.-Integr. Manuf.*, vol. 49, pp. 426–435, 2018.
- [34] C. Dong, H. Liu, W. Yue, and T. Huang, “Stiffness modeling and analysis of a novel 5-DOF hybrid robot,” *Mechanism Mach. Theory*, vol. 125, pp. 80–93, 2018.
- [35] M. Griffis and J. Duffy, “Global stiffness modeling of a class of simple compliant couplings,” *Mechanism Mach. Theory*, vol. 28, no. 2, pp. 207–224, 1993.
- [36] N. Ciblak and H. Lipkin, “Asymmetric Cartesian stiffness for the modelling of compliant robotic systems,” in *Proc. Int. Des. Eng. Tech. Conf. Comput. Inf. Eng. Conf.*, 1994, pp. 197–204.
- [37] J. Li and I. Kao, “Grasp stiffness matrix-fundamental properties in analysis of grasping and manipulation,” in *Proc. IEEE/RSJ Int. Conf. Intell. Robots Syst., Hum. Robot Interact. Cooperative Robots*, 1995, pp. 381–386.
- [38] T. Pigoski, M. Griffis, and J. Duffy, “Stiffness mappings employing different frames of reference,” *Mechanism Mach. Theory*, vol. 33, no. 6, pp. 825–838, 1998.
- [39] S. Howard, M. Žefran, and V. Kumar, “On the 6×6 Cartesian stiffness matrix for three-dimensional motions,” *Mechanism Mach. Theory*, vol. 33, no. 4, pp. 389–408, 1998.
- [40] J. S. Przemieniecki, *Theory of Matrix Structural Analysis*. Chelmsford, MA, USA: Courier Corporation, 1985.
- [41] H. R. Choi, W. K. Chung, and Y. Youm, “Stiffness analysis and control of redundant manipulators,” in *Proc. IEEE Int. Conf. Robot. Automat.*, 1994, pp. 689–695.
- [42] I. Kao and C. Ngo, “Properties of the grasp stiffness matrix and conservative control strategies,” *Int. J. Robot. Res.*, vol. 18, no. 2, pp. 159–167, 1999.
- [43] S.-F. Chen, “The spatial conservative congruence transformation for manipulator stiffness modeling with coordinate and noncoordinate bases,” *J. Robot. Syst.*, vol. 22, no. 1, pp. 31–44, 2005.
- [44] M. Žefran and V. Kumar, “A geometrical approach to the study of the Cartesian stiffness matrix,” *J. Mech. Des.*, vol. 124, no. 1, pp. 30–38, 2002.
- [45] J. Kövecses and J. Angeles, “The stiffness matrix in elastically articulated rigid-body systems,” *Multibody Syst. Dyn.*, vol. 18, no. 2, pp. 169–184, 2007.
- [46] M. F. Metzger, N. A. F. Senan, and O. M. O’Reilly, “On Cartesian stiffness matrices in rigid body dynamics: An energetic perspective,” *Multibody Syst. Dyn.*, vol. 24, no. 4, pp. 441–472, 2010.
- [47] A. Hoenenars, C. Gosselin, P. Lambert, and J. Herder, “Consistent modeling resolves asymmetry in stiffness matrices,” *Mechanism Mach. Theory*, vol. 105, pp. 80–90, 2016.
- [48] M. P. do Carmo and J. F. Francis, *Riemannian Geometry*. Boston, MA, USA: Birkhäuser, 1992.
- [49] J. E. Marsden and T. S. Ratiu, *Introduction to Mechanics and Symmetry: A Basic Exposition of Classical Mechanical Systems*. New York, NY, USA: Springer, 1999.
- [50] J. M. Lee, *Introduction to Smooth Manifolds*. New York, NY, USA: Springer, 2013.
- [51] J. M. Lee, *Introduction to Riemannian Manifolds*. New York, NY, USA: Springer, 2018.
- [52] R. M. Murray, Z. Li, and S. S. Sastry, *A Mathematical Introduction to Robotic Manipulation*. Ann Arbor, MI, USA: CRC Press, 1994.
- [53] M. Žefran and V. Kumar, “Coordinate-free formulation of the Cartesian stiffness matrix,” in *Recent Advances in Robot Kinematics*. Dordrecht, Netherlands: Springer, 1996, pp. 119–128.
- [54] V. Portman, “Robot stiffness evaluability problem: Solution by Schur complements and collinear stiffness values,” *Mechanism Mach. Theory*, vol. 161, 2021, Art. no. 104297.

- [55] N. R. Slavkovic, D. S. Milutinovic, and M. M. Glavonjic, "A method for off-line compensation of cutting force-induced errors in robotic machining by tool path modification," *Int. J. Adv. Manuf. Technol.*, vol. 70, pp. 2083–2096, 2014.
- [56] G. Xiong, Y. Ding, and L. Zhu, "Stiffness-based pose optimization of an industrial robot for five-axis milling," *Robot. Comput.- Integr. Manuf.*, vol. 55, pp. 19–28, 2019.
- [57] C. Dumas, S. Caro, S. Garnier, and B. Furet, "Joint stiffness identification of six-revolute industrial serial robots," *Robot. Comput.- Integr. Manuf.*, vol. 27, pp. 881–888, 2011.
- [58] L. Cen and S. N. Melkote, "Effect of robot dynamics on the machining forces in robotic milling," *Procedia Manuf.*, vol. 10, pp. 486–496, 2017.
- [59] L. Cen and S. N. Melkote, "CCT-based mode coupling chatter avoidance in robotic milling," *J. Manuf. Processes*, vol. 29, pp. 50–61, 2017.
- [60] A. Klimchik, A. Pashkevich, D. Chablat, and G. Hovland, "Compliance error compensation technique for parallel robots composed of non-perfect serial chains," *Robot. Comput.- Integr. Manuf.*, vol. 29, no. 2, pp. 385–393, 2013.
- [61] K. Kronander and A. Billard, "Passive interaction control with dynamical systems," *IEEE Robot. Autom. Lett.*, vol. 1, no. 1, pp. 106–113, Jan. 2016.
- [62] N. Figueroa and A. Billard, "Locally active globally stable dynamical systems: Theory, learning, and experiments," *Int. J. Robot. Res.*, vol. 41, no. 3, pp. 312–347, 2022.
- [63] K. Yanget al., "Enhanced stiffness modeling and identification method for a cable-driven spherical joint module," *IEEE Access*, vol. 7, pp. 137875–137886, 2019.
- [64] N. Boumal, B. Mishra, P.-A. Absil, and R. Sepulchre, "Manopt, A Matlab toolbox for optimization on manifolds," *J. Mach. Learn. Res.*, vol. 15, no. 42, pp. 1455–1459, 2014. [Online]. Available: <https://www.manopt.org>



Tengyu Hou received the B.S. degree in mechanical engineering from Shanghai Jiao Tong University (SJTU), Shanghai, China, in 2020. He is currently working toward the Ph.D. degree in mechanical engineering from Shanghai Jiao Tong University (SJTU), Shanghai.

His research interests include theoretical kinematics and dynamics, and robotic machining.



Ye Ding (Member, IEEE) received the Ph.D. degree in mechanical engineering from Shanghai Jiao Tong University, Shanghai, China, in 2011.

From 2011 to 2012, he was a Post-Doctoral Scholar with the University of Bremen, Bremen, Germany, from 2011 to 2012, supported by the Alexander von Humboldt Foundation. In 2013, he joined the School of Mechanical Engineering, Shanghai Jiao Tong University, where he is currently a Professor. His research interests include robotics and intelligent machining technology. Dr. Ding is an Associate Editor of the

Science China Technological Sciences.



Xiangyang Zhu (Member, IEEE) received the B.S. degree in automatic control from the Nanjing Institute of Technology, Nanjing, China, in 1985, and the M.Phil. degree in instrumentation engineering and the Ph.D. degree in control engineering, both from Southeast University, Nanjing, China, in 1989 and 1992, respectively.

From 1993 to 1994, he was a Post-Doctoral Research Fellow with the Huazhong University of Science and Technology, Wuhan, China. He joined the Department of Mechanical Engineering, Southeast

University, as an Associate Professor, in 1995. Since 2002, he has been with the School of Mechanical Engineering, Shanghai Jiao Tong University, Shanghai, China, where he is currently the Chair Professor and the Director of the Robotics Institute. He has authored or coauthored more than 200 articles in international journals and conference proceedings. His research interests include robotic manipulation planning, neuro-interfacing and neuro-prosthetics, and soft robotics.

Dr. Zhu was a recipient of a number of awards, including the National Science Fund for Distinguished Young Scholars from NSFC in 2005 and the Cheung Kong Distinguished Professorship from the Ministry of Education in 2007. He is serving on the editorial board of IEEE TRANSACTIONS ON CYBERNETICS and *Journal of Bionic Engineering*.